Pergamon

Geochimica et Cosmochimica Acta, Vol. 68, No. 12, pp. 2745–2769, 2004

0016-7037/04 $30.00 + .00

doi:10.1016/j.gca.2003.12.015

Solubility mechanisms of fluorine in peralkaline and meta-aluminous silicate glasses and in melts to magmatic temperatures

Bjorn O. Mysen,* George D. Cody, and Ashley Smith

Geophysical Laboratory, Carnegie Institution of Washington, 5251 Broad Branch Rd., NW, Washington, DC 20015, USA

(*Received September* 4, 2003; *accepted in revised form December* 16, 2003)

Abstract—Structural interaction between dissolved fluorine and silicate glass (25°C) and melt (to 1400°C) has been examined with ^{19}F and ^{29}Si MAS NMR and with Raman spectroscopy in the system Na_2O-Al_2O_3-SiO_2 as a function of Al_2O_3 content. Approximately 3 mol.% F calculated as NaF dissolved in these glasses and melts. From ^{19}F NMR spectroscopy, four different fluoride complexes were identified. These are (1) Na-F complexes (NF), (2) Na-Al-F complexes with Al in 4-fold coordination (NAF), (3) Na-Al-F complexes with Al in 6-fold coordination with F (CF), and (4) Al-F complexes with Al in 6-fold, and possibly also 4-fold coordination (TF). The latter three types of complexes may be linked to the aluminosilicate network via Al-O-Si bridges.

The abundance of sodium fluoride complexes (NF) decreases with increasing Al/(Al + Si) of the glasses and melts. The NF complexes were not detected in meta-aluminosilicate glasses and melts. The NAF, CF, and TF complexes coexist in peralkaline and meta-aluminosilicate glasses and melts.

From ^{29}Si-NMR spectra of glasses and Raman spectra of glasses and melts, the silicate structure of Al-free and Al-poor compositions becomes polymerized by dissolution of F because NF complexes scavenge network-modifying Na from the silicate. Solution of F in Al-rich peralkaline and meta-aluminous glasses and melts results in Al-F bonding and aluminosilicate depolymerization.

Temperature (above that of the glass transition) affects the Q^n-speciation reaction in the melts, $2Q^3 \Leftrightarrow Q^4 + Q^2$, in a manner similar to other alkali silicate and alkali aluminosilicate melts. Dissolved F at the concentration level used in this study does not affect the temperature-dependence of this speciation reaction.

1. INTRODUCTION

Fluorine dissolved in silicate melts affects their physicochemical properties. For example, the viscosity of F-bearing silicate melts is lower than that of their F-free equivalents (Dingwell, 1987, 1989; Dingwell et al., 1985). This effect is qualitatively similar to that of dissolved H_2O (Dingwell, 1987). However, the F-effects on melt viscosity depend on the silicate composition (Dingwell et al., 1985; Dingwell, 1989) and become less pronounced the less polymerized the silicate melt.

Liquidus temperature depression resulting from dissolved fluorine in the melt resembles that of dissolved H_2O (Wyllie and Tuttle, 1961; van Groos and Wyllie, 1967; Luth, 1988a). Further, the liquidus volumes of depolymerized silicate minerals expand as fluorine is dissolved (Foley et al., 1986; Luth, 1988a). This behavior is qualitatively similar to that of dissolved H_2O (Kushiro, 1969).

Melt property dependence on fluorine content has been modeled with various types of fluoride complexing in the melt. One or more of these proposed complexes might result in breakage of bridging oxygen bonds (see Carroll and Webster, 1994, for review). Breakage of bridging oxygen bonds in SiO_2-F glass to form Si-F bonds has been demonstrated by spectroscopic means (Yamamoto et al., 1983; Duncan et al., 1986). There are Raman data of SiO_2-NaF and SiO_2-AlF_3 glasses indicating that a portion of the dissolved fluorine exists in the form of Si-F bonds in such glass compositions as well, but as NaF or AlF_3 concentration increases, Na-F and Al-F bonding, respectively, becomes increasingly important (Mysen and Virgo, 1985). Alkali- and alkaline earth fluoride complexes have also been documented in melt and glass systems such as CaO-SiO_2-F (Luth, 1988b), Mg_2SiO_4-$NaAlSiO_4$-F (Foley et al., 1986), and Na_2O-CaO-SiO_2-F (Stebbins and Zeng, 2000).

In Na-aluminosilicate melts and glasses, data from both nuclear magnetic resonance (NMR) and Raman spectroscopy suggest that Si-F bonding is not important and that various combinations of Na-F, Al-F, and Na-Al-F complexing might occur instead. Schaller et al. (1992) suggested that for F-bearing glasses along the join $NaAlO_2$-SiO_2, AlF_3-type complexing with Al predominantly in sixfold coordination was the principal solution mechanism. Kohn et al. (1991), Zeng and Stebbins (2000), and Stebbins et al. (2000) concluded that although several percent of the Al may be in five- and sixfold coordination in such glasses, the dominant coordination state for Al in Al-fluoride complexes is 4. That conclusion is in general agreement with results from ab initio calculations by Liu and Nekvasil (2001).

Available information suggests, therefore, that there likely are several solution mechanisms of fluorine in silicate melts depending, perhaps, on the melt composition. These solution mechanisms would affect the melt structure differently. Some may cause silicate melt polymerization, whereas others result in melt depolymerization (see Carroll and Webster, 1994, for review of many of these models). One purpose of the present report is to clarify the relationships between silicate composition and fluorine solution mechanisms with the aid of ^{29}Si and ^{19}F magic angle spinning nuclear magnetic resonance (MAS

* Author to whom correspondence should be addressed (mysen@gl.ciw.edu).

Table 1. Composition of glasses[a].

			wt.%		
	NS80A0	NS80A2.5	NS80A5	NS80A7.5	NS80A10
SiO_2	80.84	79.93	79.02	77.95	76.02
Al_2O_3	0.00	4.28	8.27	12.38	16.02
Na_2O	18.98	15.47	12.78	9.75	7.23
Sum	99.82	99.68	100.07	100.08	99.27
			mol.%		
SiO_2	81.40	82.01	82.06	82.30	82.20
Al_2O_3	0.00	2.59	5.06	7.70	10.21
Na_2O	18.60	15.41	12.88	9.99	7.59
NBO/T[b]	0.457	0.294	0.170	0.047	−0.051
Al(Al + Si)	0.000	0.059	0.110	0.158	0.199
			wt.%		
	F3NS80A0	F3NS80A2.5	F3NS80A5	F3NS80A7.5	F3NS80A10
SiO_2	80.23	79.71	78.07	77.49	76.01
Al_2O_3	0.01	4.14	8.26	12.06	15.56
Na_2O	17.58	14.58	12.12	9.37	6.93
NaF	1.83	1.79	1.99	1.90	1.46
Sum	99.65	100.22	100.44	100.82	99.96
			mol.%		
SiO_2	80.29	80.63	80.03	80.37	80.86
Al_2O_3	0.01	2.47	4.99	7.37	9.76
Na_2O	17.08	14.32	12.06	9.43	7.16
NaF	2.62	2.59	2.92	2.82	2.22
Al/(Al + Si)	0.00	0.058	0.110	0.155	0.194

[a] From electron microprobe analysis.
[b] Calculated from composition with the assumption that Si^{4+} and Al^{3+} are in tetrahedral coordination in the glass.

NMR) spectroscopy of F-bearing glasses in peralkaline and meta-aluminous glasses (quenched melt) in the system Na_2O-Al_2O_3-SiO_2-F.

Existing data have been obtained on F-bearing glasses quenched from high-temperature melts. Application of the glass data to the structural behavior of fluorine in silicate melts at high temperature relies on the assumption that the high-temperature melt structure was quenched into the glass. This latter assumption is reasonable for qualitative and perhaps semiquantitative purposes. However, thermodynamic, rheological, and structure data document that thermodynamically, rheologically, and structurally a glass differs from melt (Urbain et al., 1982; Richet and Bottinga, 1986; Dingwell and Webb, 1990; Mysen and Frantz, 1994a,b see also Mysen, 1995, 2003, for reviews of relevant data). In the present report, possible effects of temperature on the solution behavior of F will be addressed by combining ambient-temperature NMR and Raman data with high-temperature, in-situ Raman-based melt structural studies.

2. EXPERIMENTAL METHODS

Starting compositions were between the joins Na_2O-SiO_2 and $NaAlO_2$-SiO_2 with 80 mol.% SiO_2; 0, 2.5, 7.5, and 10 mol.% Al_2O_3; and ~3 mol.% NaF. About 1 g of each F-free composition was made first from mixtures of spectroscopically pure Na_2CO_3, Al_2O_3, and SiO_2, ground under alcohol for 1 h, melted ~100°C above the individual liquidus temperatures (liquidus temperatures from Osborn and Muan, 1960), and quenched to glass. Approximately 3 mol.% NaF was added to each of these glasses, ground for another hour under alcohol, and remelted at the same temperature for another hour. These F-bearing samples were contained in sealed Pt tubing with 0.2 mm wall thickness to minimize possible F-loss from the melt at high temperature. These sealed (welded) capsules were employed to melt the F-bearing materials at ambient pressure and then quenched to glass in water. Weighing of these sealed containers + sample before and after melting was done to check if there may have been leak and consequent possible loss of material during this glass-making process.

The F-free glasses and melts will be referred to as NS80Ax, whereas the F-bearing glasses and melts will be referred to as F3NS80Ax. In both series of glasses x denotes mol.% Al_2O_3. Among these materials, NS80A0 and F3NS80A0 are nominally Al-free, NS80A2.5-A7.5 and F3NS80A2.5-A7.5 are peralkaline (Na > Al), and NS80A10 and F3NS80A10 nominally are meta-aluminous (Na = Al) when F is expressed as NaF.

The composition of these glasses was determined with a JEOL 8900 electron microprobe operating at 15 kV with 10 nAmp beam current. Analyses were conducted by rastering over 10 × 10 μm squares to avoid Na and F losses from the glasses during analysis. To evaluate in particular possible F and Na loss during electron microprobe analysis of these glasses, NaK_α and FK_α X-ray counting rates from the electron microprobe were monitored before each analysis as a function of counting time using the same 10 μm × 10 μm square raster. Counting times in excess of 120 s were needed before counting rates began to decrease appreciably. 120 s is longer than the time necessary for an individual analysis. Thus, it seems quite unlikely that these glasses experienced either Na or F loss during electron microprobe analysis. Ten separate squares were analyzed per glass sample. The analyzed glass compositions are listed in Table 1. Under the assumption that all Al^{3+} is in tetrahedral coordination in the F-free glasses, their degree of polymerization, NBO/T, is negatively correlated with Al/(Al + Si) (Table 1).

Glass and melt samples were examined by NMR and Raman spectroscopy. All NMR experiments were carried out using a Varian-Chemagnetics Infinity Solid-state NMR spectrometer with a static field of ~7.05 T. Fluorine (^{19}F) NMR was performed under fast MAS conditions (26 KHz) using a 2.5-mm outer diameter double resonance probe tuned to 282 MHz. The fluorine NMR spectra were referenced using a pure NaF standard.

Many of the components within the 2.5-mm probe used for ^{19}F NMR spectroscopy are fabricated from Teflon. To remove signal from the Teflon, a background suppression pulse sequence was used wherein signal from spins that experience less than a $\pi/4$ pulse is removed. For these experiments, a 3 μs $\pi/2$ pulse was employed. Tests with standards showed that complete removal of the fluorine background was achieved.

Silicon (^{29}Si) NMR experiments were performed at a MAS frequency of 7.0 KHz in a 7.5-mm double resonance probe. The excitation frequency is 59.6 MHz. A 1.5-μs pulse width (corresponding to a ~30° tip angle) was used with a 1000-s recycle delay.

Raman spectroscopy was employed to examine the structure of high-temperature silicate melts. This method was used because its probe frequency is many orders of magnitude greater than the oxygen exchange frequency among structural units in silicate melts at magmatic temperatures (McMillan et al., 1992). In comparison, high-temperature NMR spectroscopy of silicate melt is difficult because the oxygen exchange frequencies at high temperatures are such that multiple oxygen exchanges occur over the signal acquisition time (Farnan and Stebbins, 1990).

Raman spectra of both 25°C glasses and high-temperature melts were obtained with a Dilor XY confocal microRaman spectrometer using the 514 nm line of an Ar^+ ion laser for sample excitation. The laser power was several hundred mW at the sample. The Raman system was equipped with a cryogenic Thompson Model 4000 charge-coupled detector (CCD) for signal detection. High-temperature Raman spectra were recorded with the sample heated in a microheater (Mysen and Frantz, 1992; Richet et al., 1994). The temperature precision was ±2°C and the temperature gradient across the sample ≤4°C (Richet et al., 1994). A room-temperature spectrum was acquired before and after the sequence of high-temperature spectra to ascertain whether sample composition changed during high-temperature spectroscopy (see Mysen, 1997, for details of this method). The high-temperature acquisition sequence was started from the highest temperature (1100–1400°C). The temperature was then lowered in 100°C temperature intervals. Acquisition time was typically 60 s/CCD window, and two windows were needed to record the frequency region of first-order Raman scattering. All the spectra were corrected for temperature-dependent Raman scattering efficiency using the algorithm of Long (1977).

3. RESULTS

3.1. NMR Spectroscopy

3.1.1. ^{19}F MAS NMR

The ^{19}F MAS NMR spectra of the five F-bearing glasses are shown in Figure 1. The sharp peak near −120 ppm, present in all the spectra, most likely results from a small amount of a C-F complex. The source of the carbon to form such complexes is a small fraction of CO_2 (probably < 0.1–0.2 wt.%) that remains dissolved in the F-free glasses after melting of the original Na_2CO_3-Al_2O_3-SiO_2 starting compositions at ambient pressure. The CO_2-solubility in silicate melts of this kind likely is on the order of 0.1 wt.% (Pearce, 1964).

The ^{19}F NMR spectra consist of peaks near −220, −190, −170, and −145 ppm (Fig. 1). Their intensity varies systematically with glass composition. In the spectrum of Al-free F3NS80A0 glass, the dominant peak is at −220 ppm. This spectrum resembles that of F-bearing N4S glass ($Na_2O \cdot 4SiO_2$) from the study of Zeng and Stebbins (2000). They also reported a dominant peak at −220 ppm and a very weak peak near −140 ppm. A 20× vertical expansion (intensity) of the spectrum of F3NS80A0 glass may indicate a very weak peak near −140 ppm (shaded region in insert in Fig. 1), but this peak is significantly weaker than in the spectrum of the F-bearing N4S glass of Zeng and Stebbins (2000). Their N4S composition is essentially identical to F3NS80A0 except that the N4S sample has ~40% more F than F3NS80A0. This difference in F content may account for the different intensity in this frequency regime in the spectrum reported here (Fig. 1) and that of Zeng and Stebbins (2000). The −220 ppm remains in all spectra of peralkaline glasses although its intensity decreases markedly as the Al content increases. The −220 ppm peak is not observed in the ^{19}F NMR spectrum of F3NS80A10 glass.

With increasing Al content, a broad band consisting of a peak near −170 and one −190 ppm appears. A shoulder appears near −145 ppm for composition F3NS80A5. This shoulder evolves into a strong peak in the ^{19}F spectrum of F3NS80A10 glass.

Fluorine-19 spectra have been reported for some glasses at or near the SiO_2-$NaAlO_2$ join. One of these glasses is F-bearing $NaAlSi_3O_8$ (Zeng and Stebbins, 2000). The meta-aluminous composition, F3NS80A10, is slightly more silica-rich [Si/(Si + Al) = 0.8] than $NaAlSi_3O_8$ composition [Si/(Si + Al) = 0.25]. The $NaAlSi_3O_8$ sample (Zeng and Stebbins, 2000) contained ~8 times more F than F3NS80A10 glass. This difference notwithstanding, the two main peaks in both spectra are those near −145 and −190 ppm although the relative intensities of these two peaks in the present study (Fig. 1) and in that of Zeng and Stebbins (2000) differ. That difference most likely reflects the different fluorine contents of the two glasses.

The ^{19}F NMR spectra were fitted to peaks of gaussian line shape to gain a measure of the relative abundance of fluoride complexes giving rise to these peaks. Examples of such fits for F3NS80A0, F3NS80A5, and F3NS80A10 composition glasses are shown in Figure 2 with all the fitted NMR parameters summarized in Table 2. The relative areas of the individual peaks from the fitted spectra are shown in Figure 3.

The −220 ppm peak intensity decreases rapidly as the glasses become aluminous diminishing from 100% to ~20% of the total area between Al/(Al + Si) = 0 (F3NS80A0) and Al/(Al + Si) = 0.15 (F3NS80A7.5) (Fig. 3). There is no evidence for a peak at this frequency above the background scatter in the spectrum of the meta-aluminous glass, F3NS80A10 (Fig. 1). The intensity of the two bands near −170 and −190 ppm increases with increasing Al/(Al + Si) for all the aluminous samples (Fig. 3). The band near −145 ppm is visually evident in spectra with Al/(Al + Si) ≥ 0.1 (F3NS80A5), and shows an increase in relative intensity with increasing Al/(Al + Si) (Fig. 3). A band in this region cannot be resolved above the background in the ^{19}F spectrum of the least aluminous of the Al-bearing glasses, F3NS80A2.5 (see Fig. 1).

The four peaks in the ^{19}F MAS NMR spectra may be assigned to four different fluorine sites in the glasses. The −220 ppm peak is the main peak in Al-free glass (Fig. 1), and also exists in the spectra of F3NS80A2.5, F3NS80A5, and F3NS80A7.5 glasses. Its frequency is nearly coincident with that of crystalline NaF (−225 ppm, e.g., Kreinbrink et al., 1990; Miller, 1996), and can be assigned to F-bearing complexes in the glass with Na-F bonding (Zeng and Stebbins, 2000). This peak is marked as NF in Table 2 and Figures 2 and 3. Its decreasing abundance with increasing Al/(Al + Si) is consistent with decreasing activity of Na^+ as the melts become more polymerized and more aluminous. Whether or not there is oxygen in this complex cannot be determined from the ^{19}F NMR spectra. This possibility is, however, not inconsistent with the NMR data.

There may also be a very weak band near −140 ppm in the F3NS80A0 glass spectrum. This peak could possibly be assigned to a very small fraction (<1–2%) of Si-F bonding (see Zeng and Stebbins, 2000). The band is, however, so weak that

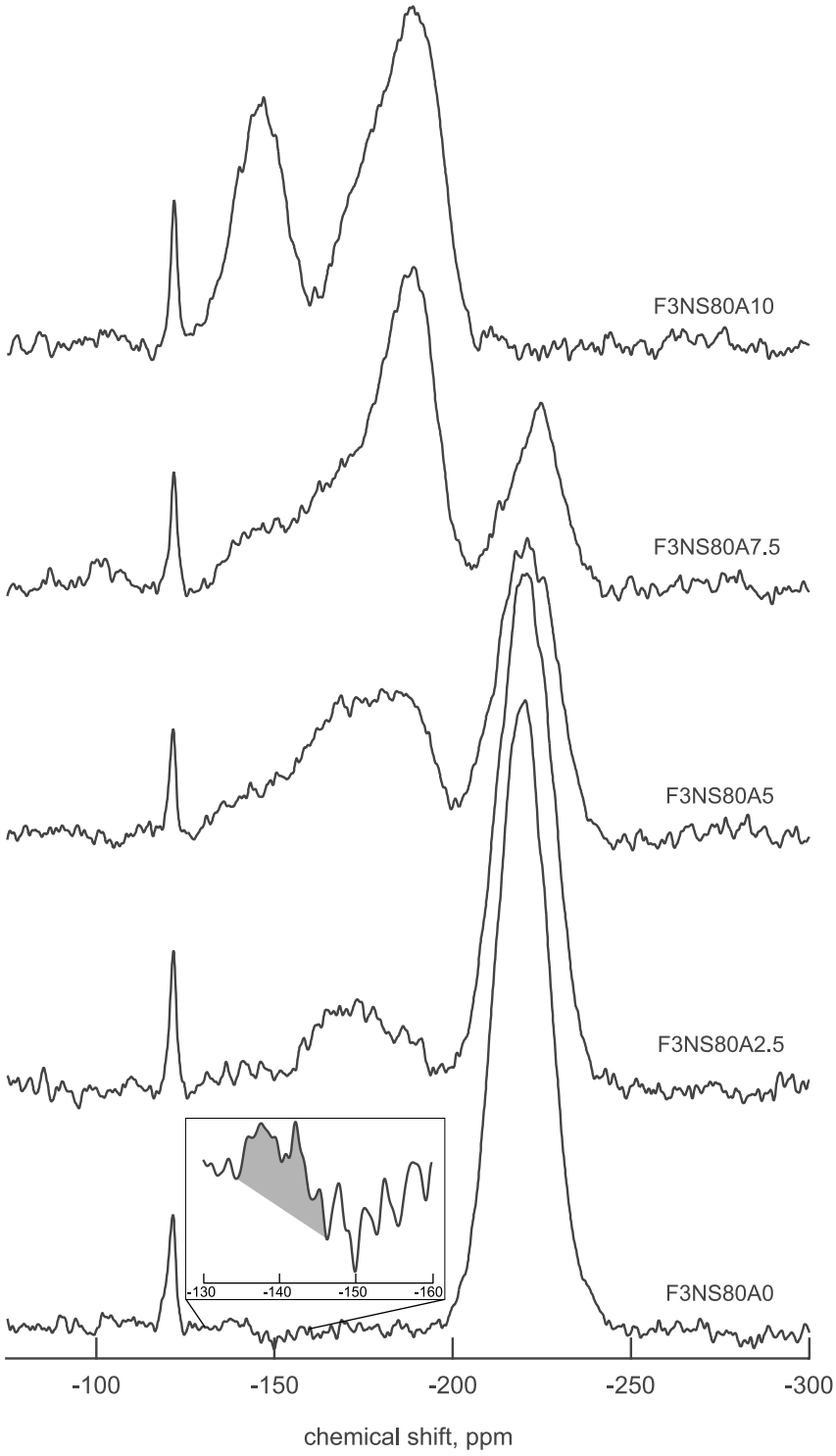

Fig. 1. ^{19}F MAS NMR spectra, normalized to total area, of F-bearing glasses as indicated on figure. Insert in −130 to −160 ppm region of spectrum of F3NS80A0 glass is expanded vertically by a factor of 20 relative to the complete F3NS80A0 spectrum. Shaded region in insert is that where there may be a small intensity increase that could be assigned to $^{[6]}$F-Si bonding (see text for detailed discussion of this feature).

the existence of Si-F bonds in F3NS80A0 glass is not certain (Fig. 1).

The peaks at −145, −170, and −190 ppm in the ^{19}F NMR spectra occur only in Al-bearing glasses (Table 2; Fig. 1) and are likely, therefore, to reflect some form of Al-F bonding (Kohn et al., 1991; Schaller et al., 1992; Stebbins et al., 2000; Liu and Nekvasil, 2001; Liu and Tossell, 2003). The exact nature of the Al-containing fluoride species (−145, −170, and

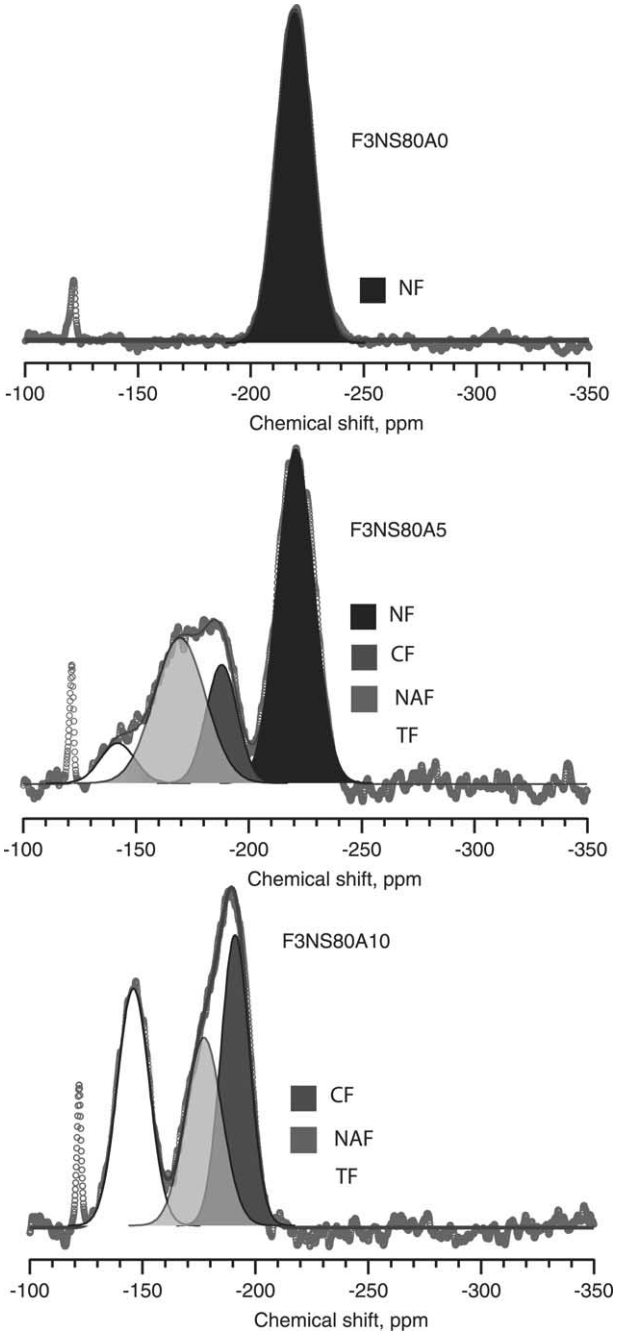

Fig. 2. Examples of curve-fitted ^{19}F MAS NMR spectra (from Fig. 1). Line parameters from all fits are given in Table 2. See text for discussion of NF, CF, NAF, and TF notations.

−190 ppm peaks) has been evaluated by comparing ^{19}F NMR glass spectra with those of possible crystalline complexes (Schaller et al., 1992; Zeng and Stebbins, 2000) and by ab initio calculations (Tossell, 1993a; Liu and Nekvasil, 2001; Liu and Tossell, 2003). Liu and Tossell (2003) concluded that no Al-F complex where all F-atoms were terminal could account for any of these bands. That conclusion would exclude AlF_3-like complexes, for example. Schaller et al. (1992) and Zeng and Stebbins (2000) suggested that the fluoride complex giving rise to the −145 ppm peak may have a topaz-like structure. Liu and Tossell (2003) in their calculations of possible Na-Al-F complexes, also concluded that the band in the −145 ppm region could be assigned to a topaz-like structure, but with, perhaps, one or two unshared F atoms. This was because the chemical shift of topaz (where all F is corner-shared) was found to be near −128 ppm. The presence of terminal F causes this peak to shift to more negative values (Liu and Tossell, 2003). Available information is, therefore, consistent with the −145 ppm being assigned to a topaz-like structure, and this structure is referred to as TF in Table 2 and Figures 2 and 3. Whether or not there is bridging oxygen linking this complex to the aluminosilicate structure is uncertain. One or two bridging oxygen per tetrahedrally coordinated, F-bonded Al^{3+} results in only 2–3 ppm shift of the ^{19}F spectra (Liu and Tossell, 2003). Such oxygen linkage is, therefore, possible.

The peak near −170 ppm (referred to as NAF in Figs. 2 and 3 and Table 2) has been ascribed to Al-F-Al groups perhaps similar to AlF_3 or to chiolite (Schaller et al., 1992; Zeng and Stebbins, 2000). Liu and Tossell (2003), on the other hand, suggested that corner-shared fluoride complexes with fourfold coordinated Al to F could also account for this band. There may also be one or more bridging oxygen between this fluoride complex and the aluminosilicate network. In this model, F becomes increasingly deshielded the larger the F/O ratio of the Al-tetrahedra. Absent Na^+, an Al-O-F-Al corner-shared complex with F/O = 0.33 yields ^{19}F shift of −171 ppm in the Liu and Tossell (2003) calculations. Our samples, do, however, contain Na. One Na cation near a corner-shared Al-O-F-Al complex causes a shift of ~9 ppm (Liu and Tossell, 2003). Deshielding of the F-atom by Na is also consistent with the NMR results of Kiczenski and Stebbins (2002). Thus, the band near −170 ppm in Na_2O-Al_2O_3-SiO_2-F glasses could be assigned to mixed Al-O-F-Al tetrahedra with F/O between 0.33 (1 F and 3 O per Al) and 1 (2 F and 2 O per Al).

The peak near −190 ppm (Fig. 1) has been assigned to a cryolite-like complex (Schaller et al., 1992; Zeng and Stebbins, 2000). The ^{19}F shift of crystalline cryolite is near −191 ppm (Schaller et al., 1992). Liu and Nekvasil (2001) and Liu and Tossell (2003), from their ab initio calculations, also concluded that this peak most likely was due to cryolite-like complexes. Oxygen bridging of this fluorine complex to the aluminosilicate network is consistent with the ^{19}F shift (Liu and Tossell, 2003). We retain that interpretation, and refer to this peak as CF in Table 2 and Figures 2 and 3.

3.1.2. ^{29}Si MAS NMR

The ^{29}Si-NMR spectra of the F-free and F-bearing glasses are shown in Figure 4. The spectrum of the F-free NS80A0 glass exhibits two nearly equally intense peaks near −107.5 and −93.0 ppm, respectively (Fig. 4A). This spectrum is identical to published ^{29}Si-NMR spectra of glasses of similar composition (Maekawa et al., 1991a; Buckermann et al., 1992). Increasing Al/(Al + Si) (and increasing degree of polymerization-see Table 1) results in decreasing intensity of the −93 ppm peak relative to that near −107 ppm and decreasing chemical shift of the ~−107 ppm peak (Fig. 4A). The spectrum of NS80A10 glass, with a single nearly symmetric peak centered near −100 ppm, is identical to the spectrum reported by Lee and Stebbins (1999) for a glass of similar composition.

The ^{29}Si-NMR spectrum of the fluorine-bearing F3NS80A0

Table 2. NMR line parameters from ^{19}F NMR spectra of glasses.

	Chemical shift, ppm				Relative area, %			
Sample	TF[a]	NAF	CF	NF	TF	NAF	CF	NF
F3NS80A0				−220				100.00
F3NS80A2.5		−172	−190	−220		17.8 ± 0.4	1.4 ± 0.4	80.9 ± 0.5
F3NS80A5	−142	−169	−189	−221	5.6 ± 0.2	30.1 ± 0.3	15.0 ± 0.4	49.4 ± 0.4
F3NS80A7.5	−146	−172	−189	−223	7.22 ± 0.5	29.6 ± 0.6	38.6 ± 0.6	14.7 ± 0.4
F3NS80A110	−146	−177	−191		33.2 ± 0.5	30.2 ± 0.2	36.6 ± 0.7	

[a] Band designations as in Figure 2 and 3. See also text for further discussion.

glass shows the same −107 ppm peak as the spectrum of the F-free equivalent, NS80A0 (Fig. 4 A,B). This peak shifts to less negative values with increasing Al/(Al + Si) similar to that in the spectra of the F-free glasses. It reaches −102.5 ppm for the most Al-rich sample, F3NS80A10, compared with −100 ppm in the ^{29}Si spectrum of the F-free NS80A10 glass. As in the spectra of F-free glasses, the shoulder near −93 ppm in the spectrum of the Al-free F3NS80A0 glass diminishes in intensity with increasing Al/(Al + Si).

The ^{29}Si-NMR spectra of NS80A0 and F3NS80A0 glass were fitted to two gaussian lines (see Maekawa et al., 1991a,b, for discussion of line shapes). The curve-fitting was carried out with the commercially available software package IGOR from Wavemetrics. Unless otherwise specified in the text, line position, intensity, and width were independent variables in this routine using χ^2-minimization as the principal convergence test during curve-fitting.

The two peaks in the ^{29}Si-NMR spectrum of NS3A0 glass are near −93 and −107.5 ppm (Fig. 5; see also Table 3). These two peaks were assigned to Q^3 and Q^4 structural units, respectively, consistent with existing ^{29}Si-NMR spectra of glasses with similar Na/Si along the Na_2O-SiO_2 join (Maekawa et al., 1991a; Buckermann et al., 1992).

The shift in the peak positions with Al/(Al + Si) of the glass (Fig. 4) may reflect intensity changes of individual ^{29}Si bands associated with different number of next-nearest neighbor Al^{3+} around Si^{4+} (Lee and Stebbins, 1999). There could be up to five possible Q^4 environments with 0–4 next-nearest tetrahedrally coordinated Al^{3+}. For Q^3-units, there could be four possible combinations of next-nearest, tetrahedrally coordinated Al^{3+}. Such units will be referred to as Q^4(mAl) and Q^3(nAl), where m = 0–4 and n = 0–3.

The ^{29}Si-NMR spectra are insufficiently well resolved to conduct curve-fitting successfully to such a large number of possible bands without constraints of one or more of the line parameters (width, position, and intensity). To deal with this situation, the model developed by Lee and Stebbins (1999) to fit the ^{29}Si-NMR spectra of glasses along meta-aluminosilicate joins was used to assist in the curve-fitting of the present spectra. The starting point when fitting peaks that may be assigned to Q^4(mAl) species was the peak position and halfwidth for individual lines assigned to Q^4(mAl) (m = 0–4) by Lee and Stebbins (1999) from the ^{29}Si-NMR spectra of glasses along the join $NaAlO_2$-SiO_2. The positions of the $Q^4(0)$, $Q^4(1)$, and $Q^4(2)$ peaks fall within the frequency range of NMR intensity of the present spectra (Fig. 4). (Notations such as $Q^4(0)$, $Q^4(1)$, etc. denote species, or structural units, with the number in parentheses representing the number of next-nearest neighbor Al^{3+} to Si^{4+}. These next-nearest Al^{3+} are linked to Si^{4+} via bridging oxygen.) Peaks from Q^4(mAl) units with m >2, occur at shifts less negative than −80 ppm (Lee and Stebbins, 1999), where there is no intensity in the present spectra (Fig. 4). Q^4(mAl) species with more than two next-nearest Al^{3+} (m > 2) will not, therefore, be considered here.

A similar approach was adopted as the starting point for curve-fitting possible peaks assigned to Q^3(nAl) (n = 0–3). The peak position for $Q^3(0)$ was that defined by the spectrum of Al-free glasses (Fig. 5; Table 3). For other possible Q^3(nAl) peaks in the spectra of Al-bearing glasses, it was assumed that the deshielding of the Si nucleus by next-nearest Al was similar to that in the Q^4(mAl) units. This assumption is consistent with observations of ^{29}Si deshielding by next-nearest Al in crystalline, tecto-, sheet- and chain-silicates (see Engelhardt and Michel, 1987, for summary of those data). The relative shift of the Q^3(nAl) peaks by 1, 2, and 3 next-nearest Al was assumed, therefore, to be similar to that of 1, 2, and 3 next-nearest Al to Si in Q^4(mAl). Initially, it was also assumed that the halfwidths of the peaks assigned to Q^3(nAl) were similar to the equivalent peaks assigned to Q^4(mAl). For Q^3(nAl), the shift at the beginning of the curve-fitting was −93.0 ppm for $Q^3(0)$ (No Al). For Q^3(1–3), the shifts would be −83.0, −75.1, and −71.4

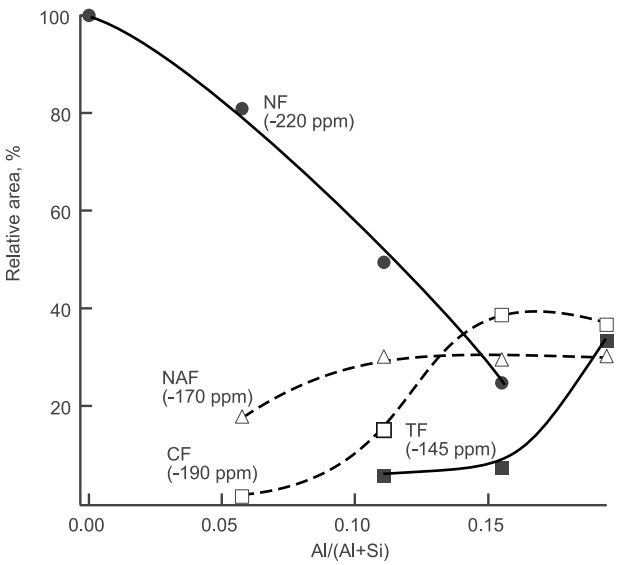

Fig. 3. Relative areas (relative abundance) of individual peaks from ^{19}F MAS NMR spectra (from curve-fitted spectra, Fig. 2 and Table 2) as a function of bulk Al/(Al + Si) of F-bearing samples. See text for discussion of NF, CF, NAF, and TF notations.

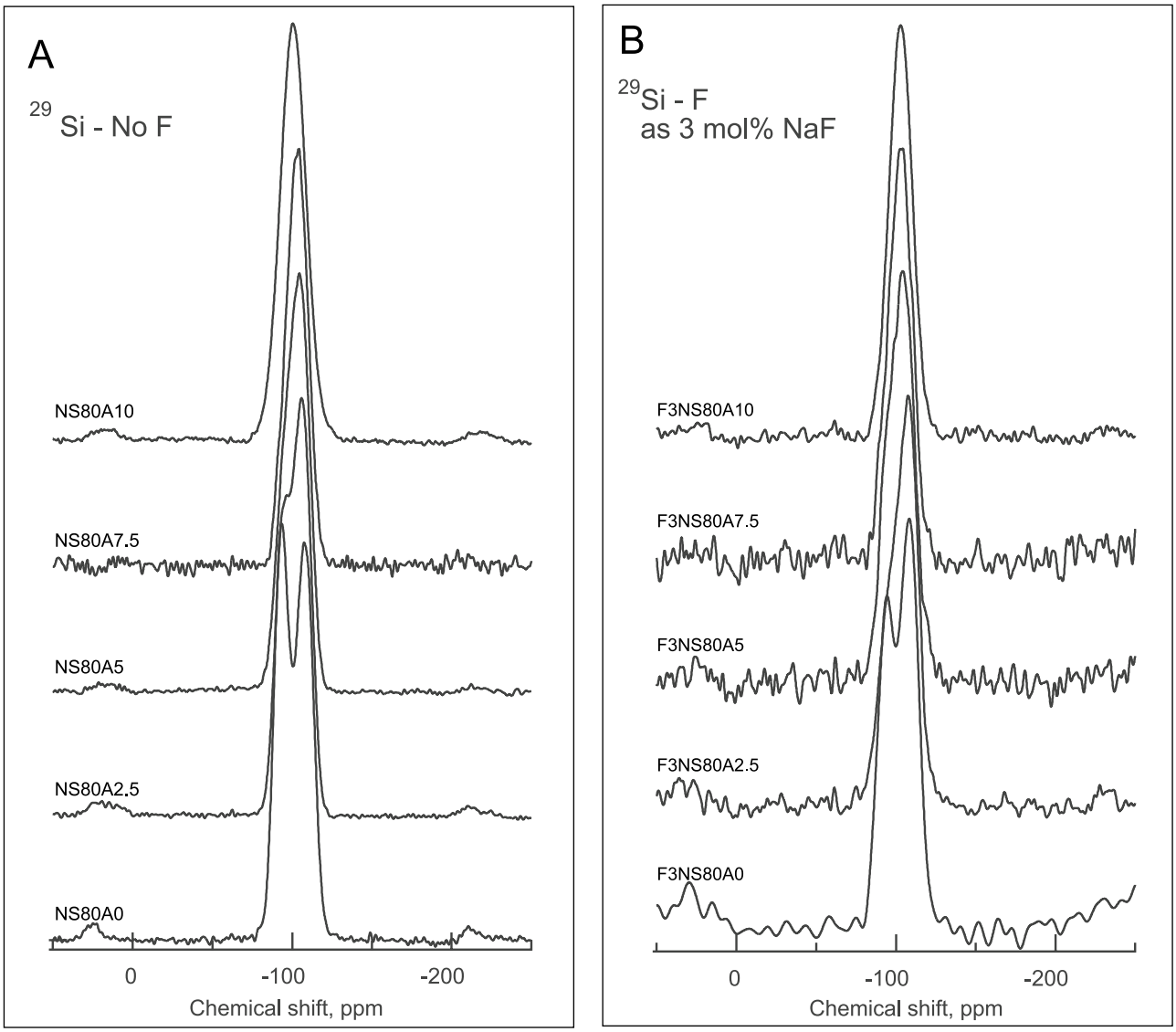

Fig. 4. ^{29}Si MAS NMR spectra, normalized to total area, of F-free (A–No F) F-bearing (B–as 3 mol.% NaF) glasses as indicated on figure.

ppm, respectively. It is immediately evident from the spectra (Fig. 4) that because there is no intensity below about −78 ppm, only $Q^3(0)$ and $Q^3(1)$ need to be considered. Peaks that could be assigned to Q^2 would have chemical shifts <-80 ppm (Murdoch et al., 1985; Engelhardt and Michel, 1987; Stebbins, 1995; Mysen et al., 2003). There is no NMR intensity in this region above the uncertainty introduced by the background scatter in the ^{29}Si-NMR spectra (Fig. 4). Thus, the maximum possible number of peaks in any of the ^{29}Si-NMR spectra is 5.

During the fitting, the line position and line width of each peak were restricted to vary within ±1 ppm because this is the approximate uncertainty in the relationships between these line parameters and the number of next-nearest Al in the ^{29}Si-NMR spectra of crystalline aluminosilicates (Engelhardt and Michel, 1987). This range in peak parameter values is also consistent with recent ^{29}Si-NMR data of glasses along the join $Na_2Si_3O_7$-$Na_2(NaAl)_3O_7$ (Mysen et al., 2003). Peak intensities were not constrained during fitting. The principal convergence criterion was minimization of χ^2.

Examples of fits obtained with this method are shown in Figure 5, with results from all the fits summarized in Table 3. The number of bands fitted to the spectra was decided on the basis of whether or not additional bands resulted in a significant decrease in χ^2. A significant decrease in χ^2 for a 3-parameter line function is ~10% (Hamilton, 1965). With this consideration in mind, only $Q^3(0)$ peaks were significant. Therefore, in the fits to the ^{29}Si-NMR spectra, only Si^{4+} in Q^4(mAl) units have next-nearest Al^{3+}.

A test of the appropriateness of this fitting approach is a comparison of the NBO/T and Al/(Al + Si) of the glasses calculated from bulk composition (Table 1) and the NBO/T- and Al/(Al + Si)-values derived from the fitted ^{29}Si-NMR spectra. The NBO/T of the glasses is equal to the abundance of Q^3-units derived from the fits to the NMR spectra because there is no Al^{3+} next-nearest neighbor to Si^{4+} in Q^3 units. The

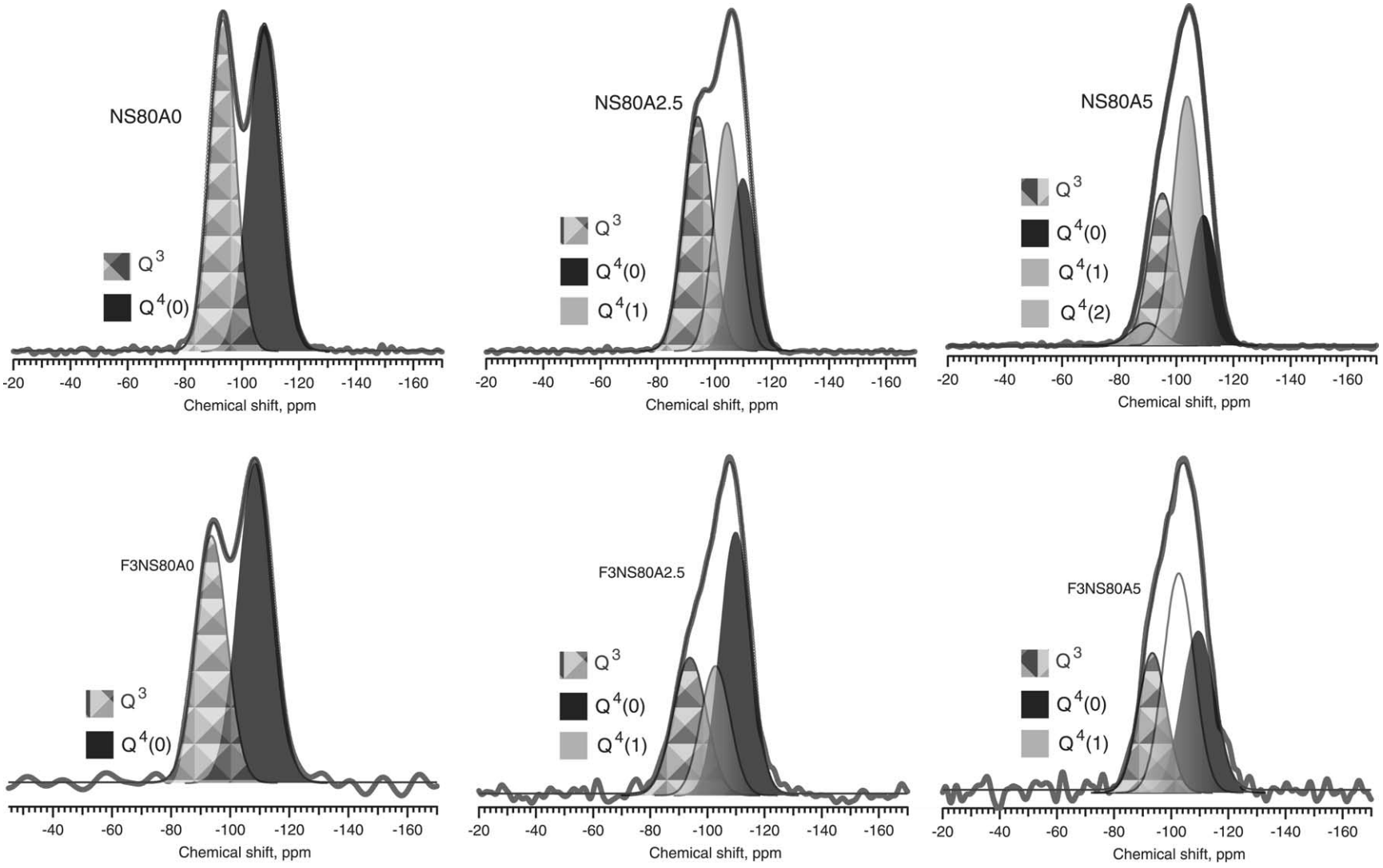

Fig. 5. Examples of curve-fitted ^{29}Si MAS NMR spectra (from Fig. 4). Line parameters from all fits are given in Table 3. See text for discussion of Q^3, $Q^4(0)$, $Q^4(1)$, and $Q^4(2)$ assignments.

Table 3. NMR line parameters from ^{29}Si NMR spectra of glasses.

	Chemical shift, ppm				Relative area, %			
Sample	Q^3 (0)	Q^4 (0)	Q^4 (1)	Q^4 (2)	Q^3 (0)	Q^4 (0)	Q^4 (1)	Q^4 (2)
NS80A0	−93.2	−107.9			46.8	53.2		
NS80A2.5	−94.3	−109.8	−104.2		39.6	25.3	35.1	0.0
NS80A5	−95.1	−109.5	−103.7	−89.5	27.7	20.9	45.8	4.6
NS80A7.5	−94.9	−109.1	−102.2	−92.8	12.8	27.3	53.2	5.3
NS80A10		−109.1	−100.4	−91.1		20.5	56.5	19.1
NS80A0F3	−93.6	−108.6			41.6	58.4		
NS80A2.5F3	−93.8	−109.8	−102.8		28.2	48.4	23.5	
NS80A5F3	−93.4	−109.5	−102.7		25.2	32.5	42.3	
NS80A7.5F3	−94.7	−109	−102.3	−91.5	16.4	27.9	47.7	6.2
NS80A10F3	−94.9	−110	−102	−92.7	3.8	22.4	63.3	8.7

NBO/T-values from the spectra of the F-free glasses thus obtained are compared with the NBO/T-values calculated from the bulk compositions in Figure 6. The two sets of NBO/T-values are in good agreement. The error in NBO/T from the NMR spectra is difficult to assess because of the highly constrained nature of the fits. Even so, observed (from NMR) and calculated (from bulk composition) NBO/T-values differ by <8%.

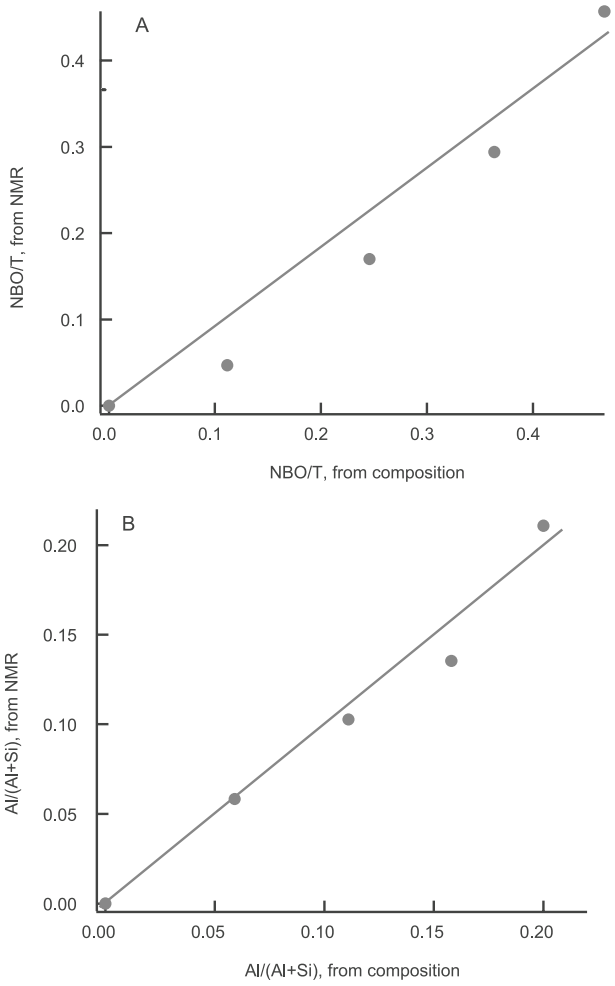

Fig. 6. Comparison of NBO/T (A) and Al/(Al + Si) (B) for F-free glasses derived from bulk composition and calculated from the ^{29}Si-NMR spectra as discussed in the text. Solid lines represent 1:1 correspondence between values.

To compare Al/(Al + Si) from the bulk composition and from the curve-fitted ^{29}NMR spectra, we first need to evaluate the distribution of Al^{3+} among the structural units in the glasses. To this end, we need to extract from the ^{29}Si spectra the concentration of both Si^{4+} and Al^{3+} in the Q^4(mAl) units. This can be accomplished as follows. For Q^4(mAl) units with 1 next-nearest Al [Q^4(1Al)], Al = 0.25Si, and for 2 next-nearest Al [Q^4(2Al)], Al = 0.5Si. Because there is no NMR intensity below about −80 ppm, more aluminous Q^4(mAl) species than Q^4(2) need no further consideration. With the assumption that Al-avoidance is obeyed, the abundance of individual Q^4(mAl) units, $X_{Q4(mAl)}$, then becomes:

$$X_{Q^4(mAl)} = Q^4(mAl) + m/4Q^4(mAl) \quad (1)$$

In Eqn. 1 Q^4(mAl) is obtained from the relative area of the peaks in the ^{29}Si-NMR spectra assigned to individual Q^4(mAl) species with m next-nearest Al^{3+} (see also Fig. 5 and Table 3). The Al/(Al + Si) of each of these units, $[Al/(Al + Si)]^{Q4(mAl)}$, is:

$$\left(\frac{Al}{Al + Si}\right)^{Q^4(mAl)} = \frac{m/4}{1 + m/4}. \quad (2)$$

The total Al/(Al + Si) of the glasses derived from the fits of the ^{29}Si-NMR spectra then becomes:

$$\frac{Al}{Al + Si} = \sum_{m=1}^{m=2} X_{Q^4(mAl)} \cdot \left(\frac{Al}{Al + Si}\right)^{Q^4(mAl)}, \quad (3)$$

where $X_{Q4(mAl)}$ is from Eqn. 1 and $[Al/(Al + Si)]^{Q4(mAl)}$ from Eqn. 2.

The Al/(Al + Si) from the ^{29}Si-NMR spectra of F-free glasses (Fig. 4) thus calculated is compared with the values calculated from bulk composition (Fig. 6B). Even though errors in the Al/(Al + Si)-values derived from the ^{29}Si-NMR spectra together with Eqns. 2 and 3 are difficult to assess because of the severe constraints imposed on the fits of these spectra, the two sets of values compare well, thus lending further credence to this approach to curve-fitting of the spectra.

The tests of the appropriateness of fits employed for the ^{29}Si-NMR spectra of F-free samples (Fig. 6) cannot be used for the spectra of F-bearing samples because the solution mechanisms of fluorine (see above) can affect both NBO/T and Al/(Al

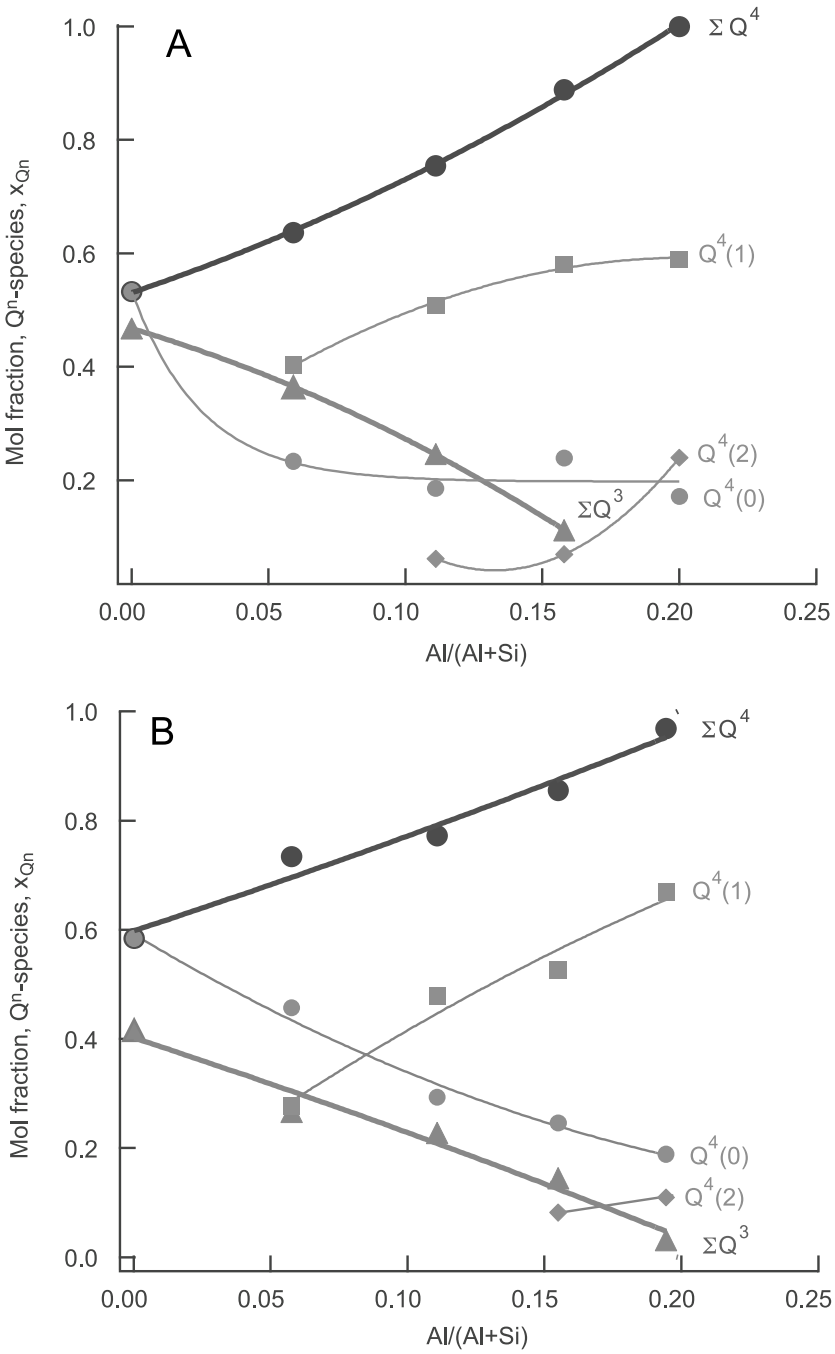

Fig. 7. Evolution of Q^n-species abundance in F-free (A) and F-bearing (B) glasses as a function of their Al/(Al + Si). In these figures, $Q^4(0)$, $Q^4(1)$, and $Q^4(2)$ represent Q^4-species with 0, 1, and 2 next-nearest Al^{3+} to Si^{4+}, $\Sigma^4 = Q^4(0) + Q^4(1) + Q^4(2)$ abundance, and ΣQ^3 the total abundance of Q^3-species. See text, in particular Eqns. 1–3, for discussion of abundance calculations.

+ Si) of the aluminosilicate. However, in light of the results of the evaluation procedure summarized in Figure 6 for the spectra of F-free samples, it is reasonable to assume that fitting of the ^{29}Si-NMR spectra of the F-bearing samples using the same approach would yield results of similar reliability.

From the curve-fitting (Table 3; Fig. 5) and the calculations via Eqns. 1–3, the evolution in abundance of Q^4(mAl) as a function of bulk melt Al/(Al + Si) is shown for the NS80A0-10 and F3NS80A0-10 glasses in Figure 7. Also shown is the total abundance of Q^4-species (ΣQ^4), which is simply the sum of abundance of the individual Q^4(mAl) species, and the Q^3-abundance, ΣQ^3. In both series of glasses, the abundance of $Q^4(0)$ (0 next-nearest Al) decreases with increasing bulk Al/(Al + Si). Qualitatively, this decrease resembles that observed for glasses along the meta-aluminosilicate join, $NaAlO_2$-SiO_2 (Lee and Stebbins, 1999) and along the join $Na_2Si_3O_7$

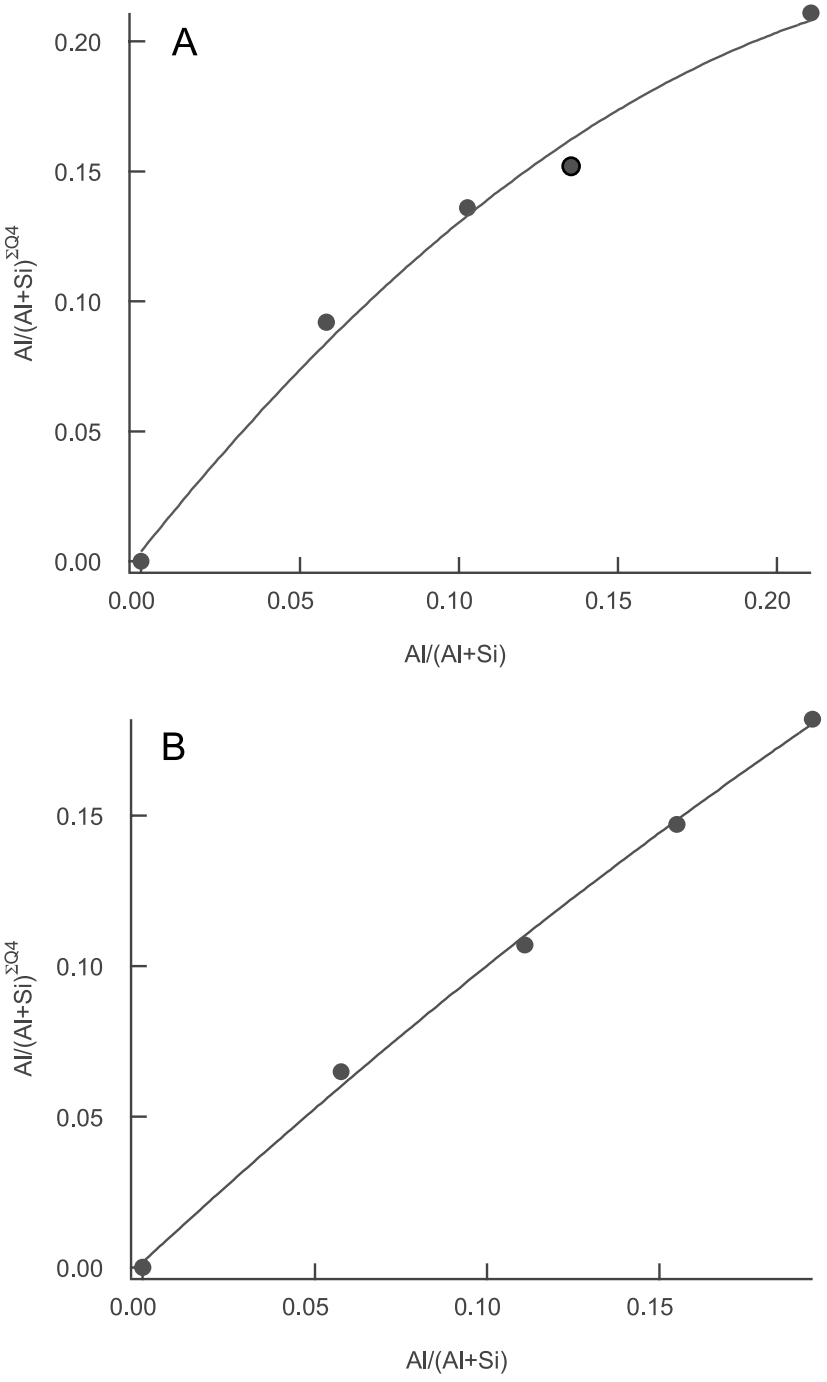

Fig. 8. Al/(Al + Si) in Q^4-species [Al/(Al + Si)$^{\Sigma Q4}$] in F-free (A) and F-bearing (B) glasses as a function of the bulk Al/(Al + Si) of the glasses. See text, in particular Eqns. 1–3, for detailed discussion of Al/(Al + Si)$^{\Sigma Q4}$ calculation.

–$Na_2(NaAl)_3O_7$ (Mysen et al., 2003). The $Q^4(1)$ species (1 nearest-neighbor Al) exists in all Al-bearing glasses (NS80A2.5-10 and F3NS80A2.5-10) with a positive correlation between its abundance and bulk melt Al/(Al + Si). The most aluminous Q^4(mAl)-species, $Q^4(2)$, is detected in F-free samples with Al-content equal to or higher than that of NS80A5 (Fig. 8A), whereas $Q^4(2)$ is not detected in the spectra of F-bearing glasses until the Al-content reaches that of F3NS80A7.5 (Fig. 7B).

The total Al/(Al + Si) of the Q^4-species, [Al/(Al + Si)]$^{\Sigma Q4}$, increases with increasing bulk Al/(Al + Si) (Fig. 7). The [Al/(Al + Si)]$^{\Sigma Q4}$ in Al-bearing, F-free samples (Fig. 8A) is higher, however, than in the F-bearing glasses of comparable bulk Al/(Al + Si) (Fig. 8B). These relations are a natural consequence of the formation of Al-F complexes in the F-bearing system as the glasses become more aluminous, thus resulting in lower Al content of the aluminosilicate network.

The ΣQ^4 and ΣQ^3 abundance trends are qualitatively con-

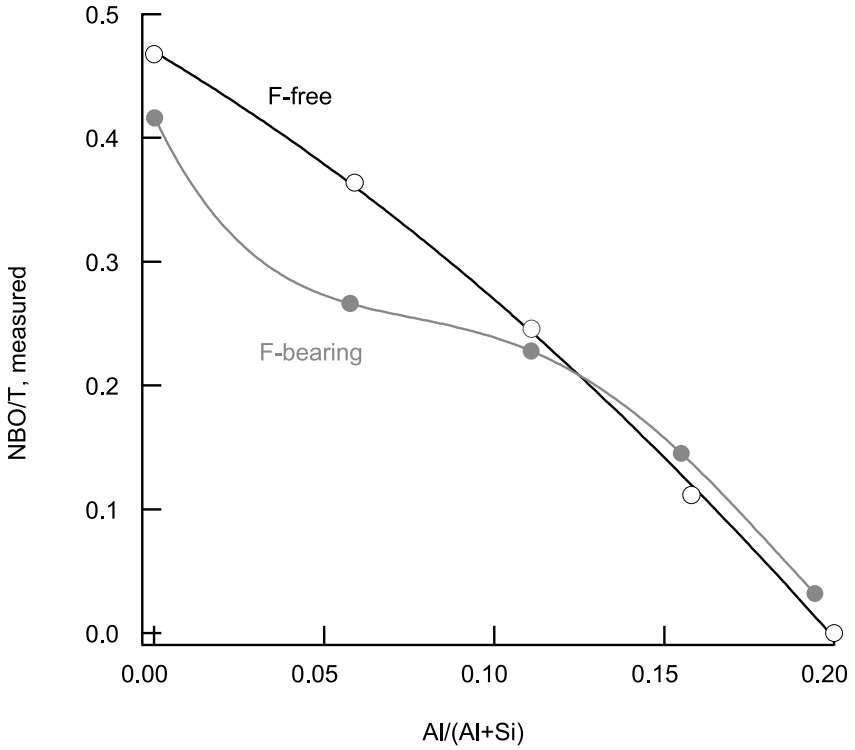

Fig. 9. Degree of polymerization, NBO/T, as F-free (open symbols) and F-bearing (solid symbols) glasses as a function of bulk Al/(Al + Si). See text for detailed discussion of NBO/T calculations.

sistent with increasing aluminosilicate polymerization as the bulk Al/(Al + Si) increases (Table 1). The ΣQ^4 in F3NS80A0 is higher and that of ΣQ^3 is lower than in the corresponding F-free glass. The rate of change of their abundance with bulk Al/(Al + Si) of F-bearing glasses also differs (Fig. 7). These abundance relations translate to the evolution of aluminosilicate glass polymerization, NBO/T, vs. bulk Al/(Al + Si) in Figure 9. Interestingly, the ^{29}Si-NMR spectrum of Al-free F3NS80A0 glass indicates polymerization of the silicate network compared with the F-free NS80A0 glass. Simply adding NaF to NS80A0 to form NaF complexes in its glass (and melt) would not result in silicate polymerization. As discussed in more detail below, polymerization of the F3NS80A0 silicate network implies that there must be some oxygen in the Na. . .F complex.

The observation that within the sensitivity of the experimental method all Al^{3+} resides in the most polymerized of the coexisting structural units (Q^4) is consistent with data from other Al-bearing glass and melt (Merzbacher et al., 1990; Maekawa et al., 1991b; Mysen et al., 1981, 2003). From crystalline aluminosilicates and numerical simulation of aluminosilicate clusters, bridging Al-O bonds typically are 5–7% longer than bridging Si-O bonds. The Al-O-Al and Si-O-Al bond angles are slightly smaller (1–3%) than Si-O-Si bond angles (Brown et al., 1969; Geisinger et al., 1985; Tossell, 1993b). One may infer, therefore, that longer bridging oxygen bonds and slightly smaller T-O-T bond angles are accommodated in fully polymerized Q^4-units in aluminosilicate melts with less energy penalty than in Q^3-units.

3.1.3. The effect of fluorine on ^{29}Si spin-lattice relaxation

The ^{19}F nucleus has a relatively large magnetic moment and at a concentration of ~3 mol.% (as NaF) would be expected to enhance the strength of the fluctuating magnetic field of the lattice, thus affecting the spin-lattice relaxation time constant, T_1, of silicon (Abragam, 1961). To explore such effects, inversion recovery experiments were performed on the F-containing glasses using a 1000-s recycle delay (Fig. 10). Note that only in the case of Al-free glass was the recovery followed to near completion. In this case, the relaxation back to equilibrium clearly is multi-exponential, a fact not surprising given the structural complexity of glasses.

The effect of increased aluminum content is revealed in Figure 10 as a progressive increase in T_1. It is not possible to derive a quantitative value for T_1 given both the multi-exponential nature of the data and the incomplete recovery exhibited by most of the samples. A coarse estimate of T_1 can be derived from the null signal (I = 0.0) time for each curve in Figure 10. Such an analysis provides estimates of ^{29}Si T_1 on the order of ~20 s for the F-bearing samples without Al (F3NS80A0) and up to ~200 s for samples with 10 mol.% Al_2O_3 (F3NS80A10). In each case these T_1-values are considerably less than those of similar composition glasses without F. The increase in T_1 with increasing aluminum content is consistent with a progressive shift of fluorine, inferred from the ^{19}F NMR data (Figs. 1–3), from Na-F complexes to Na-Al-F clusters that may be linked to and distributed within the aluminosilicate network as the glasses become more aluminous.

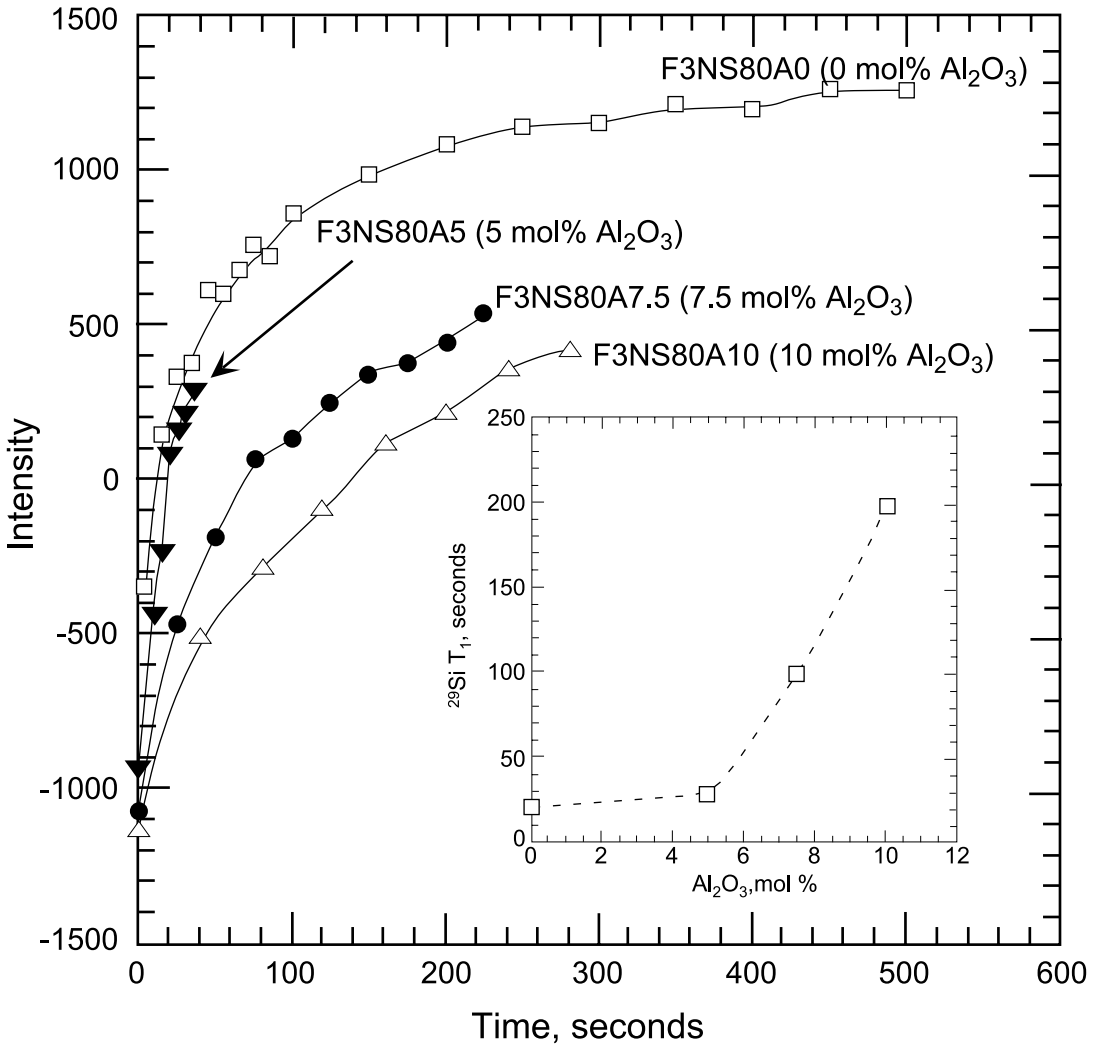

Fig. 10. Results of standard inversion recovery (180° pulse-variable delay—90° pulse-detect) experiments from F-bearing glasses as a function of their Al_2O_3 content using a 1000-s recycle delay.

3.2. Raman Spectroscopy

The Raman spectra of F-free NS80A0-NS80A10 and F-bearing F3NS80A0-F3NS80A10 series glasses in the frequency range of first-order Raman scattering show two dominant features, between 400 and 700 cm^{-1} and between 900 and 1200 cm^{-1}, respectively (Fig. 11). For both F-free and F-bearing glasses with no or low alumina contents, there is a sharp maximum near 1100 cm^{-1} with a shoulder on its high-frequency side. There is another maximum near 500 cm^{-1} also with a peak or a shoulder on its high-frequency side. The former frequency region is that of (Si,Al)-O stretch vibrations, and that between ~400 and 600 cm^{-1} is the region of (Si,Al)-O rocking and bending motions (see, for example, Furukawa et al., 1981; McMillan, 1984). The spectral region centered near 1100 cm^{-1} broadens and becomes less well resolved with increasing bulk melt Al/(Al + Si) (Fig. 11). The exact Raman frequencies in these regions depend on the types and proportions of Q^n-species in the melts and on their Si/Al-ratios (Seifert et al., 1982; Matson et al., 1986; Mysen, 1999). The spectral features in Figure 11 are similar to those observed in Raman spectra of other alkali silicate and alkali aluminosilicate glasses (Brawer and White, 1975; McMillan, 1984; Virgo et al., 1980).

Differences between F-free and F-bearing glasses have been amplified by subtracting spectra of F-free glasses from those of the equivalent F-bearing glasses (Fig. 11C). For glasses with $Al_2O_3 \leq 5$ mol.%, the differences between the pairs of spectra are quite small, reflecting most likely only subtle changes in Al/Si ratio and Q^n-species abundance resulting from interaction between dissolved fluorine and the aluminosilicate network. For glasses with higher Al_2O_3 contents, there are changes in the intermediate frequency region between ~600 cm^{-1} and 900 cm^{-1} (shaded regions in Fig. 11C). There is an intensity growth near 800 cm^{-1}, which is likely due to stretching vibrations of $^{[4]}$Al-F bonds in analogy with $^{[4]}$Al-O bond stretching in this frequency range (Sato et al., 1991). This interpretation is consistent with the interpretation of ^{19}F NMR spectra of these glasses (Figs. 1–3; Table 2), suggesting increasing importance

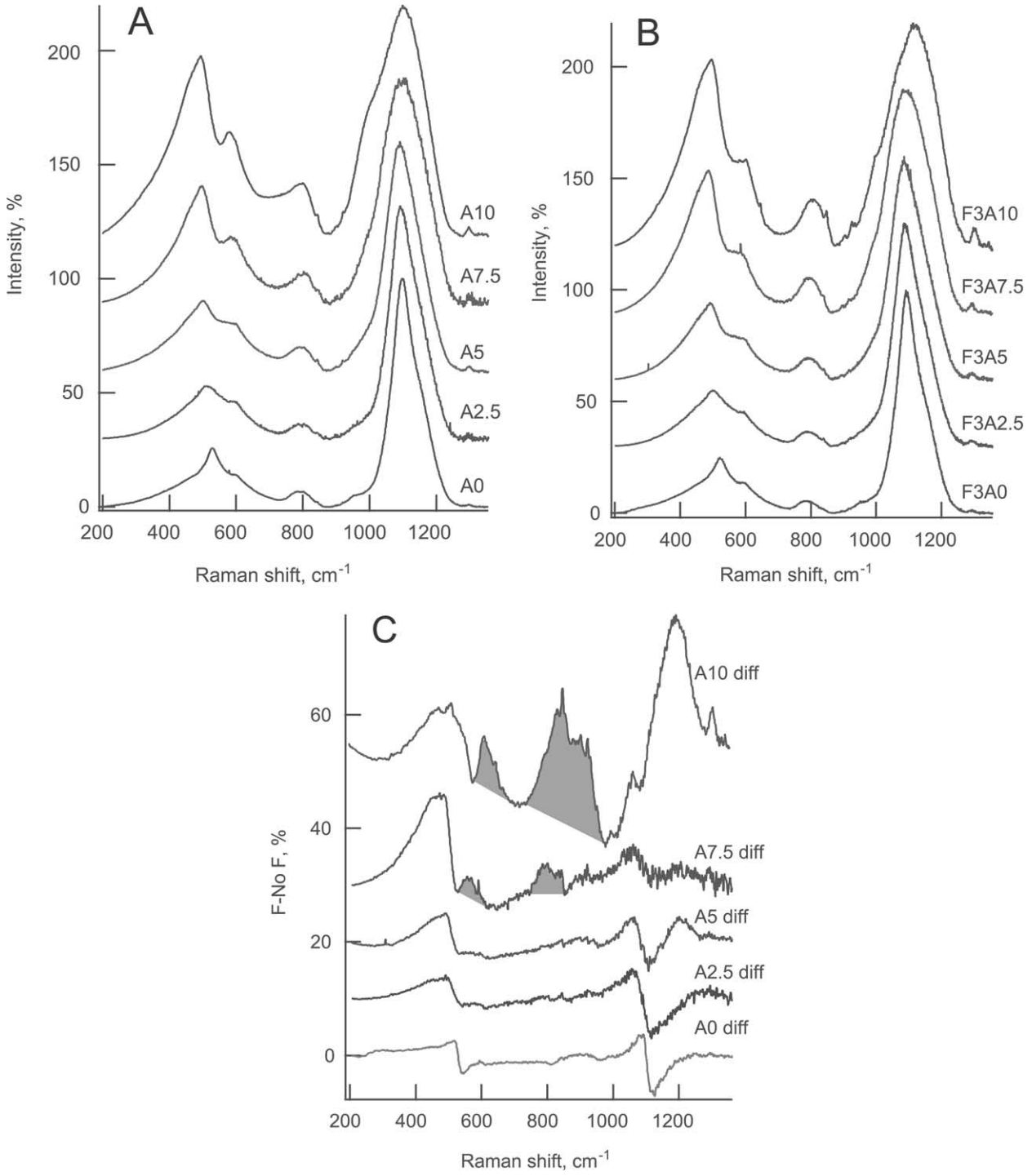

Fig. 11. Raman spectra obtained at 25°C of F-free (A) and F-bearing (B) glasses in the frequency region of first-order Raman scattering. In panel A, A0, A2.5, A5, A7.5, and A10 denote compositions NS80A0, NS80A2.5, NS80A5, NS80A7.5, and NS80A10, respectively. In panel B, F3A0, F3A2.5, F3A5, F3A7.5, and F3A10 denote compositions F3NS80A0, F3NS80A2.5, F3NS80A5, F3NS80A7.5, and F3NS80A10, respectively. All spectra in (A) and (B) are normalized to 100% intensity, where 100% represents that data point within each spectrum of the highest intensity. The spectra are offset for clarity. Panel C: Difference spectra between F-bearing (B) and F-free (A) spectra with the individual difference spectra offset for clarity. A0 diff = spectrum F3A0 − spectrum A0; A2.5 diff = spectrum F3A2.5 − spectrum A2.5; A5 diff = spectrum F3A5 − spectrum A5; A7.5 diff = spectrum F3A7.5 − spectrum A7.5; and A10 diff = spectrum F3A10 − spectrum A10. See text for discussion of shaded regions in C.

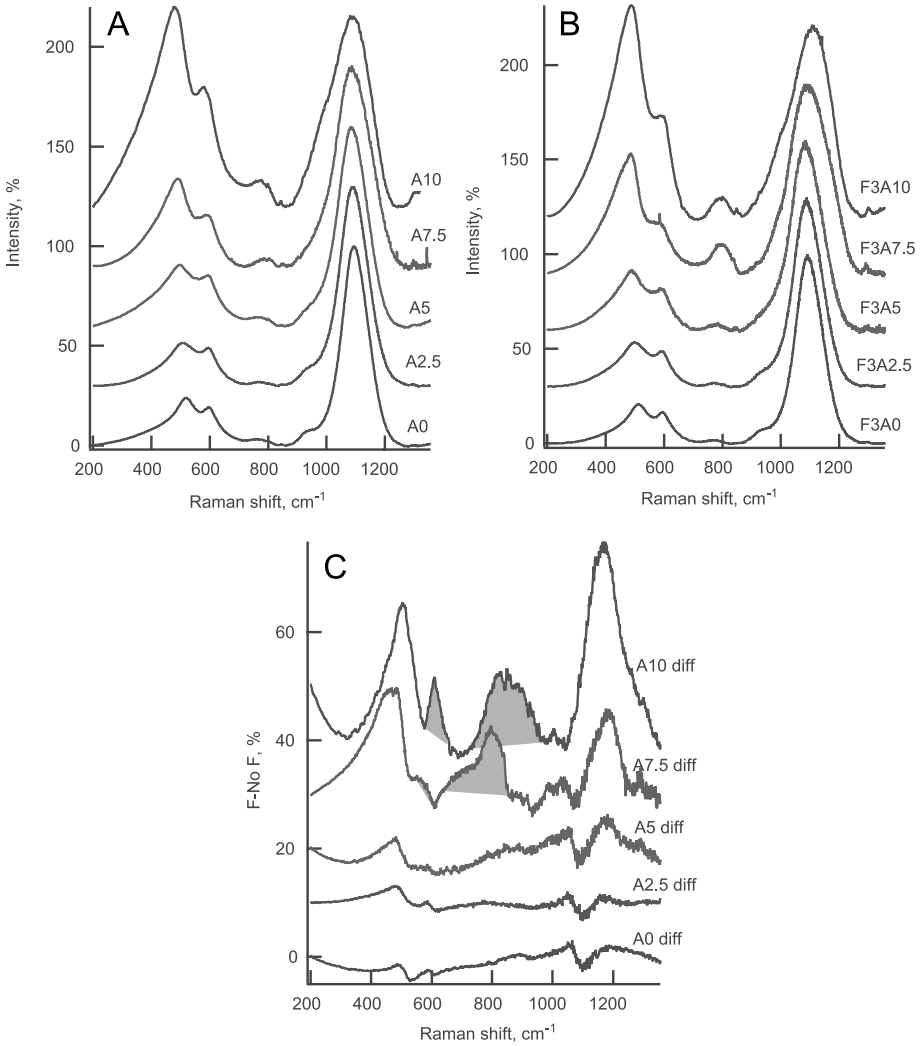

Fig. 12. Raman spectra obtained at 1000°C of F-free (A) and F-bearing (B) melts (supercooled liquids) in the frequency region of first-order Raman scattering. In panel A, A0, A2.5, A5, A7.5, and A10 denote compositions NS80A0, NS80A2.5, NS80A5, NS80A7.5, and NS80A10, respectively. In panel B, F3A0, F3A2.5, F3A5, F3A7.5, and F3A10 denote compositions F3NS80A0, F3NS80A2.5, F3NS80A5, F3NS80A7.5, and F3NS80A10, respectively. All spectra in (A) and (B) are normalized to 100% intensity, where 100% represents that data point within each spectrum of the highest intensity. The spectra are offset for clarity. Panel C: Difference spectra between F-bearing (B) and F-free (A) spectra with the individual difference spectra offset for clarity. A0 diff = spectrum F3A0 − spectrum A0; A2.5 diff = spectrum F3A2.5 − spectrum A2.5; A5 diff = spectrum F3A5 − spectrum A5; A7.5 diff = spectrum F3A7.5 − spectrum A7.5; and A10 diff = spectrum F3A10 − spectrum A10. See text for discussion of shaded regions in C.

of Al-F bonding with increasing Al content of the glass (see discussion above). At least one of these F-complexes, denoted NAF in Figures 2 and 3, is characterized by fourfold coordination of F around Al, consistent with the Raman intensity increase near 800 cm^{-1} (Fig. 11C).

The intensity increase near 600 cm^{-1} (Fig. 12C) occurs in a frequency range similar to that observed for molten cryolite (Gilbert et al., 1975) and is considered consistent with $^{[6]}$Al-F bonding in these Al-rich, F-bearing glasses. The existence of both the CF and TF complexes suggested from the ^{19}F NMR spectra of these glasses (−145 and −190 ppm peaks in the ^{19}F spectra; see Figs. 1–3; Table 2) are consistent with this interpretation of the Raman spectra.

Raman spectra were also recorded to temperatures up to 1400°C (for some of the compositions) at 100°C intervals. Thus, spectra were taken both below and above the glass transition temperature and to temperatures slightly above the liquidus for these compositions (see Osborn and Muan, 1960, for liquidus phase relations in the system Na_2O-Al_2O_3-SiO_2). Examples of spectra taken at 1000°C are shown in Figure 12A, B with difference spectra (F-free subtracted from F-bearing) shown in Figure 12C. The high-temperature spectra resemble those of their equivalent 25°C glasses (Figs. 11 and 12), suggesting, therefore, no major changes in the structure of these materials as they are transformed from a glass to a liquid.

It has been suggested that higher-order Raman scattering may contribute a few percent intensity to spectra of silicate and aluminosilicate melts at magmatic temperatures (Daniel et al.,

1995; McMillan et al., 1994). However, within the several percent background scatter in the present data, higher-order Raman bands were not detected in the present spectra.

The difference spectra at 25°C and 1000°C (Figs. 11C and 12C) also resemble one another. In particular for samples with Al_2O_3 ≤5 mol.% the difference between 25°C and 1000°C spectra is negligible (Figs. 11C and 12C). For materials with Al_2O_3 ≥7.5 mol.%, the intensity increase centered near 800 cm^{-1}, as in the 25°C spectra, is evident. The peak near 600 cm^{-1} remains strong in the difference spectrum of 10 mol.% Al_2O_3 samples, whereas this peak is weaker in the 7.5 mol.% Al_2O_3 differences spectra of 1000°C melt (Figs. 11C and 12C). This difference in intensity may be because of temperature-dependent changes in abundance of fluoride complexes in melts vs. glass or simply because Raman scattering intensity is intrinsically temperature-dependent (Long, 1977). This temperature-dependence differs for different oscillators.

The high-frequency portion of the Raman spectra (~900–1300 cm^{-1}) was fitted to 3–5 gaussian bands, after correction for instrumental background and temperature-dependent Raman scattering intensity (Long, 1977). The curve-fitting was carried out with the IGOR software package from Wavemetrics. In these fits, position (Raman shift), band width, and band intensity were treated as independent variables and minimum χ^2 was used as the principal convergence criterion.

In the fits to spectra of peralkaline glasses and melts, ≤4 gaussian lines satisfy the data (e.g., Fig. 13 A,B,E,F). The band near 950 cm^{-1} (light shading in Fig. 13) is assigned to (Si,Al)-O^- (O^-–nonbridging oxygen) vibrations in Q^2 structural units, that near 1100 cm^{-1} (dark shading in Fig. 13) to (Si,Al)-O^- vibrations in Q^3. The band near 1150 cm^{-1} (vertical hachure) is assigned to (Si,Al)-O° (O° –bridging oxygen) in Q^4 units. These assignments are consistent with the ^{29}Si-NMR spectra of the glasses discussed above and are also in agreement with existing Raman data of other silicate glasses and melts (McMillan and Wolf, 1995; Mysen, 1995).

The 1050 cm^{-1} band [which shifts to lower frequency with increasing Al/(Al + Si) of the glasses and melts] fitted to all the spectra of peralkaline alkali silicate and alkali aluminosilicate glasses and melts (marked with horizontal hachure in Fig. 13) also has been reported in Raman spectra of vitreous silica as well as in Raman spectra of other alkali- and alkaline earth-silicate and –aluminosilicate melts and glasses (Bell and Dean, 1972; Brawer and White, 1975, 1977; Furukawa et al., 1981; Mysen et al., 1982; Fukumi et al., 1990; McMillan et al., 1992; Mysen and Frantz, 1993, 1994a). One proposed assignment of this band is to Si-O° or (Si,Al)-O° vibrations in any structural unit that contains bridging oxygen, but does not need by itself to be fully polymerized (Mysen et al., 1982; Lasaga, 1982). An alternative assignment is to Si-O vibrations in Q^3 units associated with alkali metals or alkaline earths (Fukumi et al., 1990; McMillan et al., 1992). The nature of this suggested association with alkali metals was not specified. There is, however, no evidence for a second Q^3 structural unit in the ^{29}Si-NMR spectra of glasses reported here or existing in the literature (Maekawa et al., 1991a; Buckermann et al., 1992). The former assignment [(Si,Al)-O° vibration] is, therefore, the more likely of the two alternatives.

The structure of these peralkaline glasses, based on the band assignments of their Raman spectra, is, therefore, essentially the same as that from ^{29}Si-NMR of the same materials (Figs. 4 and 5; see also Table 3). There is, however, a small difference in that whereas Raman spectrometry suggests a small proportion of Q^2 structural units (950 cm^{-1} band, see Fig. 13), the ^{29}Si-NMR of these glasses is insufficiently sensitive to detect Q^2. This sensitivity limitation is because the chemical shift of ^{29}Si-NMR peaks that might be assigned to Q^2 structural units is in the −75 to −80 ppm range (Engelhardt and Michel, 1987). A few percent intensity in this frequency range of the ^{29}Si-NMR spectra (Figs. 4 and 5) cannot be isolated from the low-frequency tail of the peak assigned to Q^3 units over the background noise in these spectra.

The ^{29}Si-NMR spectrum of the meta-aluminosilicate glass, NS80A10 (Fig. 4) was interpreted consistent with a fully polymerized, three-dimensionally interconnected structure, an interpretation also consistent with existing ^{29}Si-NMR and X-ray data of glasses along the join SiO_2-$NaAlO_2$ (Lee and Stebbins, 1999; Taylor and Brown, 1979). The Raman spectrum of the same glass (Fig. 11A; upper spectrum) is identical to existing Raman spectra of glasses along the same join (Seifert et al., 1982; Neuville and Mysen, 1996). The curve-fitted high-frequency envelope of this Raman spectrum (Fig. 13C) consists of three peaks all of which can be assigned to (Si,Al)-O° (O°-bridging oxygen) in the fully polymerized three-dimensionally interconnected network of this glass (see Seifert et al., 1982, for discussion of band assignments in this frequency region of Raman spectra of glasses along the SiO_2-$NaAlO_2$ join).

The spectrum of F-bearing, 25°C-F3NS80A10 glass (Fig. 13G) is slightly different from the F-free equivalent because from a statistical perspective (Hamilton, 1965) two additional bands may be necessary (shaded in Fig. 13G). The curve-fitted ^{29}Si-NMR spectrum of F3NS80A10 glass indicates that this glass contains 3.8% Q^3 (Table 3) consistent, therefore, with the fitted peak near 1100 cm^{-1} in the Raman spectrum of this glass. There is also a weak band near 950 cm^{-1} (Fig. 13G). This band can be assigned to (Si,Al)-O^- stretching in Q^2 structural units as in the spectra of the peralkaline glasses above. However, the ^{29}Si-NMR spectrum of this glass cannot be fitted to include a peak in the −75–80 ppm range, which would be expected for Q^2 (Murdoch et al., 1985; Engelhardt and Michel, 1987; Mysen et al., 2003). The 950 cm^{-1} peak is quite weak and the absence of a corresponding peak in the ^{29}Si-NMR spectrum may due to statistically unresolvable intensity in this region (as also discussed above).

Examples of fits to the high-frequency region of Raman spectra recorded at 1000°C (in the supercooled temperature region above the glass transition temperatures of these compositions) are shown in Figure 13 (B, D, F, and H) (Line parameters resulting from the curve-fitting of the 133 spectra examined for this purpose are available from the authors upon request). The differences between these and those recorded of glass at 25°C (Fig. 13 A, C, E, and G) are relatively subtle with an intensity increase in the ~950 cm^{-1} region being the principal effect. The temperature-driven changes in these spectra are similar to that observed in high-temperature Raman spectra of other alkali silicate and alkali aluminosilicate melts (McMillan et al., 1992; Mysen and Frantz, 1992, 1993, 1994a,b).

The aluminosilicate glass and melt structure, for both F-free and F-bearing materials, may, therefore, be expressed as an equilibrium between Q^2, Q^3, and Q^4 structural units of the kind:

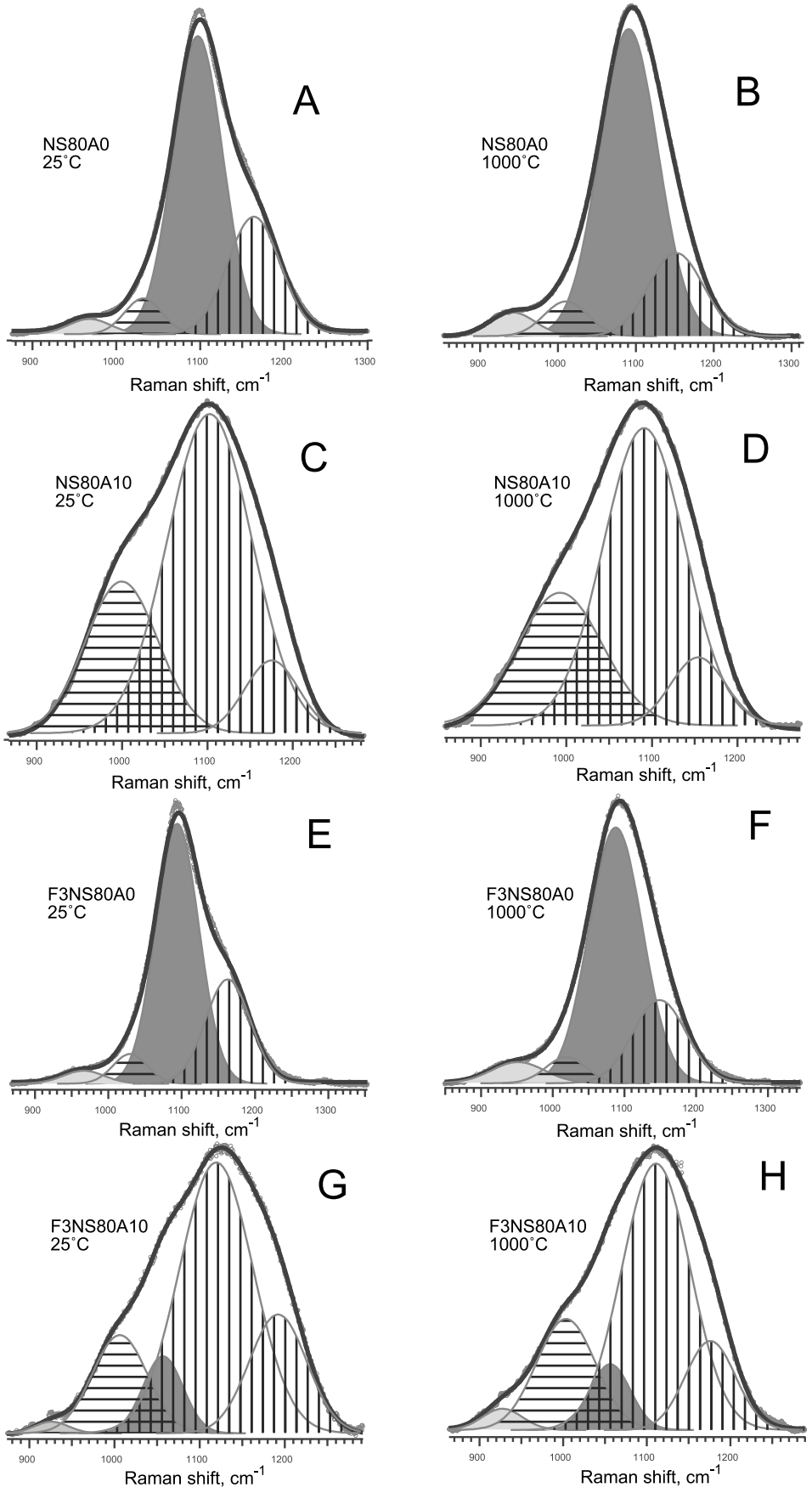

Fig. 13. Examples of Raman spectra of 25°C glasses and 1000°C melts in the frequency region on (Si, Al)-O stretch vibrations for compositions indicated. The individual lines are of gaussian shape and fitted to the spectra as discussed in the text. Also see text for discussion of shading and patterns and assignments of these bands. (Results of the curve-fitting to all the spectra examined are available from the authors upon request).

Table 4. Regression coefficients for temperature-dependent frequency of Raman bands, v = a + bT.

	950 cm^{-1} band			1050 cm^{-1} band			1100 cm^{-1} band			1200 cm^{-1} band		
	a	b	R	a	b	R	a	b	R	a	b	R
NS80A0	969 ± 1	−0.027 ± 0.002	0.97	1030.2 ± 0.8	−0.0202 ± 0.0009	0.99	1098.4 ± 0.4	−0.0070 ± 0.0005	0.97	1172 ± 3	−0.022 ± 0.003	0.89
F3NS80A0	969 ± 1	−0.017 ± 0.002	0.96	1030.7 ± 0.6	−0.0123 ± 0.0008	0.98	1094.2 ± 0.3	−0.0060 ± 0.0004	0.98	1163.3 ± 0.8	−0.013 ± 0.001	0.97
NS80A2.5	967 ± 1	−0.0117 ± 0.0008	0.97	1029.5 ± 0.4	−0.0040 ± 0.0004	0.93	1092.1 ± 0.2	−0.0028 ± 0.0002	0.96	1158.0 ± 0.6	−0.0050 ± 0.0007	0.90
F3NS80A2.5	966 ± 1	−0.0075 ± 0.0006	0.97	1032.6 ± 0.3	−0.0077 ± 0.0004	0.99	1088.7 ± 0.2	−0.0045 ± 0.0003	0.97	1155.8 ± 0.6	−0.0098 ± 0.00008	0.96
NS80A5	963 ± 1	−0.0101 ± 0.0004	0.99	1021 ± 1	−0.006 ± 0.001	0.78	1086.7 ± 0.2	−0.0033 ± 0.0002	0.97	1153.9 ± 0.5	−0.0063 ± 0.0006	0.95
F3NS80A5	965 ± 1	−0.003 ± 0.001	0.59	1029 ± 2	−0.008 ± 0.003	0.63	1085.9 ± 0.3	−0.0067 ± 0.0002	0.98	1160.5 ± 0.5	−0.0151 ± 0.0007	0.99
NS80A7.5	964 ± 1	−0.0014 ± 0.0006	0.56	1022 ± 1	−0.004 ± 0.001	0.70	1088.2 ± 0.5	−0.0044 ± 0.0006	0.89	1161.7 ± 0.4	−0.0043 ± 0.0005	0.92
F3NS80A7.5	964 ± 1	−0.0026 ± 0.0009	0.66	1028.9 ± 0.7	−0.006 ± 0.001	0.88	1088.5 ± 0.6	−0.0064 ± 0.0008	0.92	1161.4 ± 0.7	−0.009 ± 0.001	0.95

	1000 cm^{-1} band			1120 cm^{-1} band			1170 cm^{-1} band		
	a	b	R	a	b	R	a	b	R
NS80A10	1002 ± 2	−0.012 ± 0.002	0.83	1105 ± 1	−0.016 ± 0.002	0.95	1176.1 ± 0.9	−0.002 ± 0.001	0.98

	950 cm^{-1} band			1000 cm^{-1} band			1100 cm^{-1} band			1120 cm^{-1} band			1200 cm^{-1} band		
	a	b	R	a	b	R	a	b	R	a	b	R	a	b	R
F3NS80A10	929 ± 1	−0.001 ± 0.002	0.18	1006.0 ± 0.3	−0.0027 ± 0.0004	0.88	1056.0 ± 0.3	0.0001 ± 0.0003	0.10	1121.2 ± 0.7	−0.0110 ± 0.0009	0.96	1194 ± 1	−0.017 ± 0.001	0.97

$$2Q^3 \Leftrightarrow Q^2 + Q^4 \quad (4)$$

This conclusion is entirely consistent with published NMR- and Raman-based structural data for silicate glasses and melts of compositions similar to those examined here (see Stebbins, 1995; Mysen, 1995, for reviews of such data).

The temperature-derivative of frequency of Raman bands assigned to (Si,Al)-O stretching, $\partial\nu_i/\partial T$, is constant (Table 4) and typical of the temperature-dependence of the frequency of bands assigned to Si-O stretching in alkali silicate and aluminosilicate melts (McMillan et al., 1992; Mysen and Frantz, 1994a; Mysen, 1997). A change in Al/(Al + Si) within a structural unit because of increased temperature could cause a change in $\partial\nu_i/\partial T$. Raman frequencies decrease with increasing Al/(Al + Si) (Seifert et al., 1982). Changes in $\partial\nu_i/\partial T$ with temperature were not observed. There is, therefore, no evidence in the high-temperature Raman spectra for temperature-dependence of Al-distribution among the coexisting structural units. We also conclude that the types of fluoride complexes remain the same. If this were not the case, one would expect that the Al/(Al + Si) in the aluminosilicate structures would change thus resulting in a change of $\partial\nu_i/\partial T$. It must be cautioned, however, that the sensitivity of $\partial\nu_i/\partial T$ of individual Raman bands to variations in Al/(Al + Si) is not well known. Thus, the precision of this conclusion cannot be ascertained.

Raman band intensity in spectra of 25°C glass was calibrated in terms of mol fraction of structural units by combining Raman and ^{29}Si-NMR spectral data of the glasses (Mysen and Frantz, 1993; Mysen and Cody, 2001). In this method, the mol fractions of Q^4, Q^3, and Q^2 structural units, X_{Q4}, X_{Q3}, and X_{Q2}, are obtained from the equations:

$$X_{Q3}/X_{Q2} = (\theta_{Q3}/\theta_{Q2}) \cdot (A_{Q3}/A_{Q2}), \quad (5)$$

$$2X_{Q2} + X_{Q3} = \mathrm{NBO/T}, \quad (6)$$

and

$$X_{Q4} + X_{Q3} + X_{Q2} = 1. \quad (7)$$

In Eqn. 5, A_{Q2} and A_{Q3} are the integrated Raman intensities of the 950 and 1100 cm^{-1} bands. The X_{Q3}/X_{Q2}-ratio is from the ^{29}Si-NMR spectra, and the θ_{Q3}/θ_{Q2}-ratio is the calibration factor that relates Raman intensity to concentration of structural units. The NBO/T of the 25°C glasses is obtained from their ^{29}Si-NMR spectra. The mol fraction of Q^4 structural units is the sum of the abundance of the individual Q^4(mAl) species from the ^{29}Si-NMR spectra as summarized above (see also Eqn. 1).

Raman intensity ratios (A_{Q3}/A_{Q2}) were used rather than absolute Raman intensities because absolute Raman intensities are intrinsically temperature-dependent (Long, 1977). By using ratios of intensities of bands from similar vibrations in Q^3 and Q^2 structural units (950 and 1100 cm^{-1} bands), this intrinsic temperature dependence is likely to be similar so that the intensity ratio may depend only on the abundance ratio of the Q^3 and Q^2 structural units, X_{Q3}/X_{Q2}. This suggestion was tested by measuring A_{Q3}/A_{Q2} of glasses as a function of temperature at temperatures below that of the glass transition. Below the glass transition, the abundance of structural units is not dependent on temperature (see also Dingwell and Webb, 1990). For the present compositions, A_{Q3}/A_{Q2} does not vary with temperature below that of the glass transition within the uncertaintyof the data, which is similar to observations from other aluminosilicate glasses (Mysen, 1999; Mysen et al., 2003). In such a case, the calibration ratio, θ_{Q3}/θ_{Q2}, is independent of temperature and can be applied in Eqn. 5 together with Eqns. 6 and 7 to compute the abundance of Q^4, Q^3, and Q^2 structural units for each of the compositions as a function of temperature at temperatures above the glass transition.

Two additional issues require attention before Eqns. 5–7 can be used to derive the abundance of the structural units from high-temperature Raman spectra: (1) It is assumed that NBO/T of F-bearing and F-free glasses does not vary with temperature. This is likely a good assumption because there is no evidence for formation or disappearance of structural units or fluoride complexes, identified in 25°C glasses, as these glasses are transformed to melts. Further, if the proportion of fluoride complexes, all of which involve interaction with Na and Al

from the aluminosilicate network, varied with temperature, this would most likely result in changes in Al/(Al + Si) of the aluminosilicate structural units. That, in turn, would likely cause changes in $\partial \nu_i/\partial T$. This was not observed. Thus the assumption that NBO/T does not vary with temperature appears reasonable. (2) Whereas the Raman spectra indicate that Q^2 units are present in the glasses and melts (Figs. 11–13), Q^2 units were not detected in the ^{29}Si-NMR spectra for the reasons discussed above. Their proportions from the Raman spectra were obtained, therefore, with the aid of ^{29}Si-NMR spectra of glasses along the join $Na_2Si_3O_7$-$Na_2(NaAl)_3O_7$ where Mysen et al. (2003) reported θ_{Q3}/θ_{Q2}-ratios as a function of Al/(Al + Si). These θ_{Q3}/θ_{Q2}-ratios were used in the present study to convert integrated Raman intensities to mol fractions of Q^3 and Q^2 units with the aid of Eqns. 5 and 6 and the mol fraction of Q^4 units from Eqn. 7. This procedure introduces a small error because we employ the NBO/T calculated from the ^{29}Si-NMR spectra of the present glasses based entirely on the abundance of Q^3 units from those spectra (see Figs. 2 and 3; Table 3). However, a small fraction of the intensity of the Q^3 peaks in the ^{29}Si-NMR spectra is actually due to Q^2. The difference between the actual value of NBO/T and the one derived from the abundance of Q^3 species from the ^{29}Si-NMR spectra alone equals the mol fraction of Q^2 units included in the relative integrated intensity of the peak assigned to Q^3-species in the NMR spectra. Although this error is difficult to determine accurately, from the abundance of Q^3 and Q^2 units (see results of these calculations in Fig. 14) derived with the NBO/T of the melt from the Q^3 abundance from the ^{29}Si-NMR spectra (Table 3) and the θ_{Q3}/θ_{Q2}-ratios from the $Na_2Si_3O_7$-$Na_2(NaAl)_3O_7$ system, the actual NBO/T is probably underestimated by between 5% and 10% (relative).

The abundance of Q^4, Q^3, and Q^2 species, X_{Q4}, X_{Q3}, and X_2, as a function of temperature is shown in Figure 14 with the samples from F-free glasses and melts as open symbols and those from F-bearing samples as closed symbols. In all cases, there is a temperature interval from room temperature to 400–600°C (depending on composition), where the concentration of structural units does not depend on temperature. The temperature at which unit abundance becomes temperature-dependent, T_m, probably is near that of the glass transition temperature (Mysen et al., 2003). For composition NS80A0, for example, the calorimetric glass transition temperature is 497°C (Knoche et al., 1994). From the data in Figure 14, the abundance of structural units in NS80A0 does not depend on temperature between 25°C and ~500°C. Their abundance is temperature-dependent at higher temperatures.

Above T_m, X_{Q2} and X_{Q4} are positively correlated with temperature, whereas X_{Q3} decreases (Fig. 14) for both F-free and F-bearing samples. In other words, the equilibrium constant for equilibrium (4),

$$K_4 = X_{Q2} \cdot X_{Q4}/(X_{Q3})^2, \quad (8)$$

increases with temperature (Fig. 15). Linear regression of 1/T vs. ln K_4 through the high-temperature portion ($T > T_m$) of the data yields an enthalpy, ΔH, for equilibrium (4) with values in the 10–15 kJ/mol range (Table 5). This range is typical for alkali aluminosilicate melts (Mysen, 2003). Within the uncertainty of the data, there is no evidence to suggest that the presence of fluorine affects this equilibrium significantly.

4. SOLUTION MECHANISMS AND PROPERTIES OF F-BEARING SILICATE MELTS

The ^{19}F NMR data of depolymerized, Al-free melts such as F3NS80A0, are consistent with F forming (Na + F)-bearing complexes, NF (Figs. 1 and 2). The ^{29}Si-NMR data from F-free and F-bearing NS80A0 and F3NS80A0 glasses are consistent with polymerization of the silicate when these NaF complexes are formed (e.g., Fig. 5). The high-temperature Raman data of the same glasses and melts (Figs. 12 and 13) indicate that similar solution mechanisms operate in the melts. Because F was added to the starting materials as NaF, formation of a simple NaF complex cannot, however, affect the silicate network. Increased silicate network polymerization (Fig. 9) under such circumstances requires that some oxygen originally in the silicate network must be involved in the NF complexes. Several O/F-ratios in the NF complex are possible, but this ratio cannot be determined from the NMR or Raman data. For simplicity, consider the simplest possible such complex, Na_3OF to illustrate how formation of such a complex causes silicate network polymerization:

$$2Q^3 + 2Na^+ + NaF \Leftrightarrow 2Q^4 + Na_3OF. \quad (9)$$

The greater the O/F ratio in such a complex, the more polymerization of the silicate network will take place.

The solution mechanism illustrated in Eqn. 9 is in principle similar to that proposed by Luth (1988b) for F-solution in melts in the CaO-SiO_2-F system where, however, Ca-F bonding instead of Na-F bonding was the principal form of fluoride complexing. Similar bonding was observed in mixed Na_2O-CaO-SiO_2-F glasses (Stebbins and Zeng, 2000).

In Al-bearing silicate glass, up to a total of four different types of fluoride complexes, depending on aluminosilicate composition, were inferred from the ^{19}F and ^{29}Si-NMR spectra. Raman spectroscopy suggests that there are no major changes in these complexes when the glasses are transformed to melts. These four complexes are (1) Na-F(-O) complexes (NF in Figs. 2 and 3), (2) mixed fluorine–oxygen Na-Al-F complexes with Al in fourfold coordination with corner-shared F (NAF in Figs. 3 and 4), (3) Na-Al-F complexes with Al in sixfold coordination with F (CF in Figs. 3 and 4). This complex has been referred to as a cryolite-like (Na_3AlF_6) complex in existing literature (Zeng and Stebbins, 2000). (4) Al-F complexes with Al in sixfold, and possibly also fourfold coordination (TF in Figs. 3 and 4). This structure has been referred to as a topaz-like structure [$Al_2(SiO_4)F_2$] (Schaller et al., 1992) although possibly with Si in the SiO_4 group replaced with Al and perhaps some of the oxygen replaced with F to form, for example, a complex resembling $Al_2(AlO_3F)F_2$. In such a structure, there may be Al-F bonding with Al in both fourfold and sixfold coordination with F.

The Al-bearing fluoride complexes (NAF, CF, TF) may be linked to the aluminosilicate network via bridging oxygen. Such linkage is consistent with the computational results of Liu and Tossell (2003). It is also consistent with the positive correlation between spin-lattice relaxation time, T_1, from the ^{29}Si-NMR data and the Al content of the F-bearing glasses (Fig. 11).

The Na/Al-ratio in complexes with Al-F bonding is not readily specified. It would seem likely, however, that the Na/

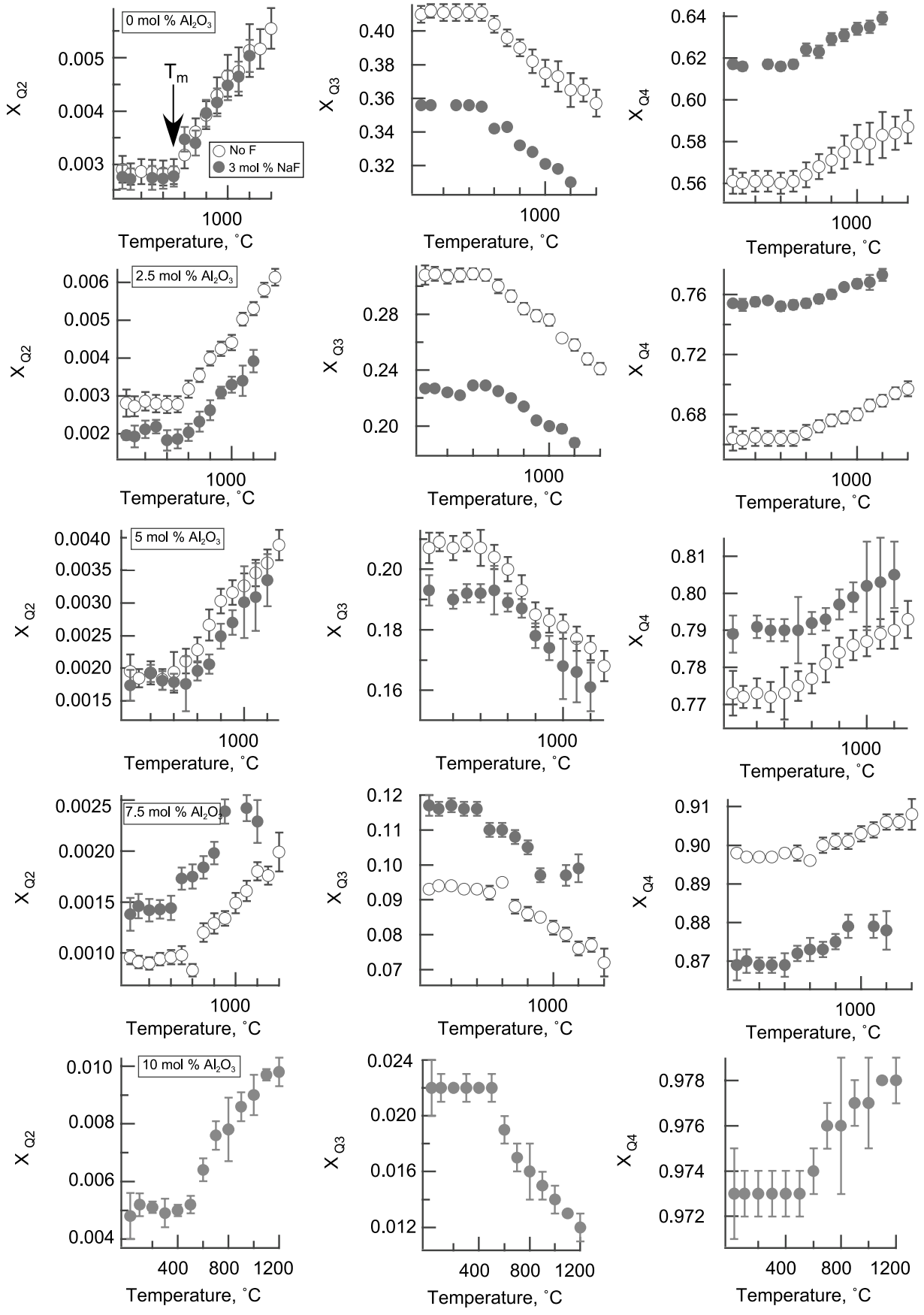
0 mol % Al2O3
Tm
No F
3 mol % NaF
2.5 mol % Al2O3
5 mol % Al2O3
7.5 mol % Al2O3
10 mol % Al2O3
XQ2
XQ3
XQ4
Temperature, ˚C
1000
400 800 1200

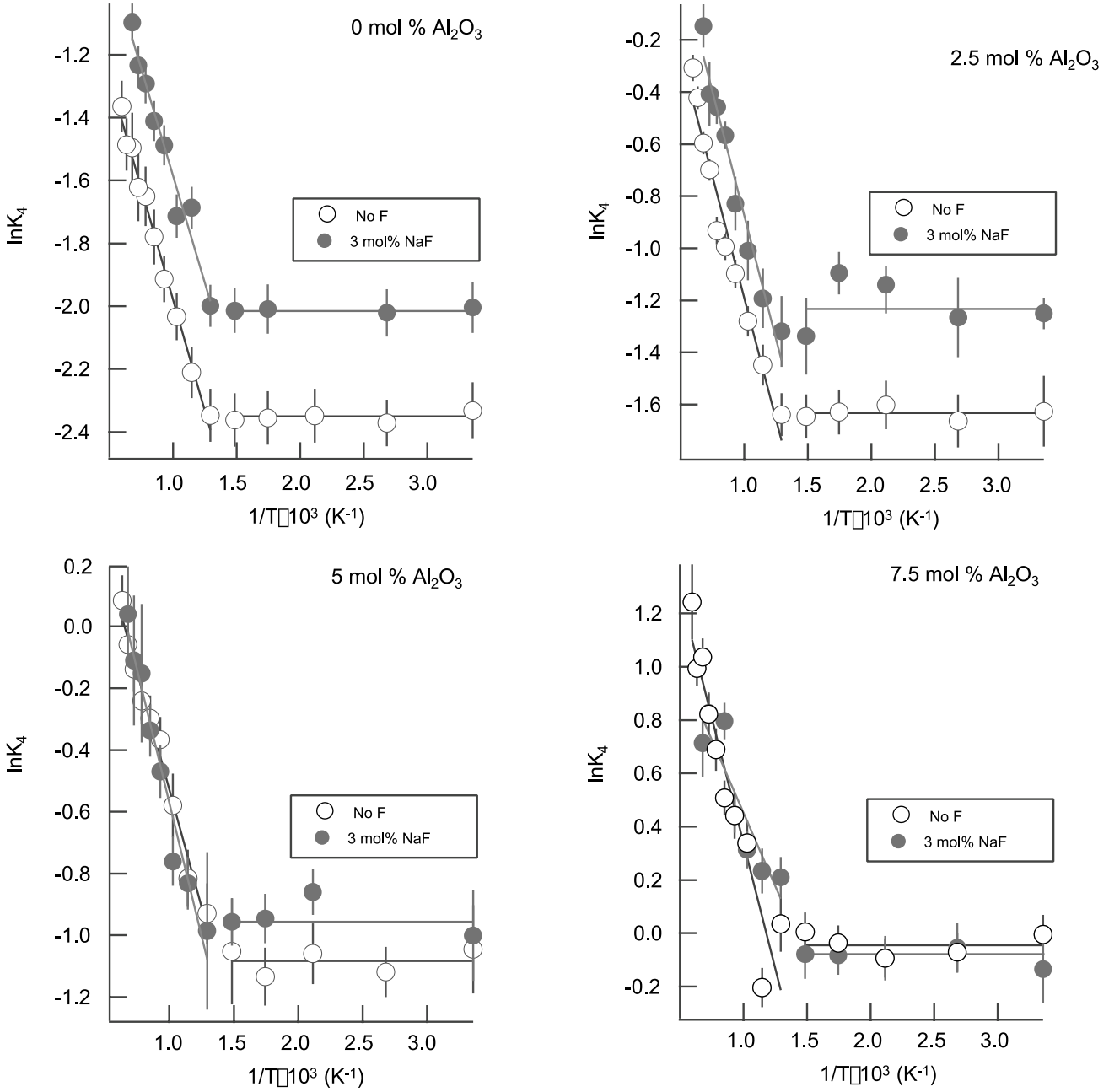

Fig. 15. Relationship between equilibrium constant for equilibrium (4) in the text, ln K_4, as a function of temperature (1/T, Kelvin) for F-free (open circles marked No F) and F-bearing (closed circles marked 3 mol.% NaF) glasses and melts. 0 mol.% Al_2O_3 show data for NS80A0 and F3NS80A0 compositions, 2.5 mol.% Al_2O_3 show data for NS80A2.5 and F3NS80A2.5 compositions, 5 mol.% Al_2O_3 show data for NS80A5 and F3NS80A5 compositions, and 7.5 mol.% Al_2O_3 show data for NS80A7.5 and F3NS80A7.5 compositions.

Fig. 14. Mol fraction of Q^2, X_{Q2}, Q^3, X_{Q3}, and Q^4, X_{Q4}, structural units as a function of temperature for F-free (open circles marked No F) and F-bearing (closed circles marked 3 mol.% NaF) glasses and melts. 0 mol.% Al_2O_3 show data for NS80A0 and F3NS80A0 compositions, 2.5 mol.% Al_2O_3 show data for NS80A2.5 and F3NS80A2.5 compositions, 5 mol.% Al_2O_3 show data for NS80A5 and F3NS80A5 compositions, 7.5 mol.% Al_2O_3 show data for NS80A7.5 and F3NS80A7.5 compositions, and 10 mol.% Al_2O_3 show data for NS80A10 and F3NS80A10 compositions. The arrow marked T_m (shown only in the diagram for compositions with 0 mol.% Al_2O_3 [NS80A0 and F3NS80A0]) denotes the temperature above which the abundance of the structural units is dependent on temperature. See detailed discussion of T_m in the text.

Table 5. Regression coefficients for the expression in $K_4 = a + b/T$ for data at $T > T_m$ in Figure 15.

Composition	a	b	ΔH (kJ/mol)	R^2
NS80A0	−0.55 ± 0.4	1419 ± 48	11.8 ± 0.4	0.99
F3NS80A0	−0.2 ± 0.1	−1361 ± 106	11.3 ± 0.9	0.96
NS80A2.5	0.7 ± 0.1	−1871 ± 130	15.5 ± 1.1	0.96
F3NS80A2.5	1.0 ± 0.1	−1897 ± 154	15.8 ± 1.3	0.96
NS80A5	1.00 ± 0.07	−1524 ± 75	12.7 ± 0.6	0.97
F3NS80A5	1.2 ± 0.1	−1729 ± 136	14.4 ± 1.1	0.96
NS80A7.5	2.2 ± 0.2	−1883 ± 220	15.6 ± 1.8	0.90
F3NS80A7.5	1.6 ± 0.2	−1100 ± 226	9.1 ± 1.9	0.89

Al-ratio of these complexes decreases as Al/(Al + Si) increases and Na/Al of the melts decreases. Formation of Na- and Al-bearing fluoride complexes may cause depolymerization of aluminosilicate melts because Al^{3+} in tetrahedral coordination in the aluminosilicate structure reacts with F to form Al-F bonds. In the process, a proportion of Na^+ required for charge-balance of tetrahedrally coordinated Al^{3+} in the aluminosilicate structure could become network-modifying, resulting, therefore, in depolymerization. This proportion of Na^+ can be equal to the fraction of Al^{3+} that reacts with F to form Al-F complexes if there is no Na in these fluoride complexes, but will be less than this amount if the fluoride complex incorporates Na, Al, and F.

Only the topaz-like complex, TF, falls in the latter category (no Na in the fluoride complex). As an example of this type of fluoride solution behavior, consider the stoichiometry of NS80A10 ($NaAlSi_4O_{10}$) aluminosilicate composition and a topaz-like structure for the fluoride complex with Al^{3+} replacing Si^{4+} where there is one oxygen bridge from the fluoride complex to the aluminosilicate network [$Al_2(AlO_3F)F_2$]. A schematic solution mechanism to form such a fluoride complex is:

$$6NaAlSi_4O_{10} + 3F_2O_{-1} \Leftrightarrow 2Al_2(AlO_3)F_2 + 6Na^+ + 4Q^3 + Q^2 + 19Q^4. \quad (10)$$

In this type of reaction, 1 Na^+ per Al^{3+} in the aluminosilicate melt is released to become a network-modifier for each Al^{3+} transformed from tetrahedral coordination in the aluminosilicate structure to form $Al_2(AlO_3)F_2$. The result is depolymerization of the silicate.

Formation of a cryolite-like complex in aluminosilicate melts such as that of composition F3NS80A10 may also result in depolymerization of the aluminosilicate network. Formation of cryolite-like complexes in aluminosilicate melts was also inferred from liquidus phase relations in hydrous quartzofeldspathic systems (Manning, 1981; Manning et al., 1980). Whether this complex exists as Na_3AlF_6, or involves oxygen bridging to the aluminosilicate network [e.g., $Na(Na_3AlF_5O)$, $Na_2(Na_3AlF_4O_2)$ and so forth] is not certain (but consistent with the data) because increasing O/F in this complex causes only a few ppm deshielding of the ^{19}F nucleus (Liu and Tossell, 2003). For simplicity, we will refer to this complex as Na_3AlF_6, but this is not meant to imply that oxygen-bearing formulations may also be consistent with the NMR data.

Depolymerization of the aluminosilicate by formation of cryolite-like complexes in the melt may take place because Na/Al differs from 1 in the cryolite stoichiometry. In meta-aluminosilicates (nominally fully polymerized melts) Na/Al = 1. For example, for each mol of Na_3AlF_6, $2Na^+$ in excess of that needed to charge-balance Al^{3+} in tetrahedral coordination in the aluminosilicate are needed. As a result, some Al^{3+} may no longer have Na^+ available for charge-balance in tetrahedral coordination.

Whether or not the Al^{3+} without Na-charge-balance remains in tetrahedral coordination or is transformed to a network-modifier, is not clear as existing structural data of peraluminous aluminosilicate melts and glasses are not conclusive. Mass-balance of the oxygen budget in such melts suggests that the formation of an Na_3AlF_6 complex also involves formation of depolymerized Q^n-species with $n \leq 3$ as illustrated with the F3NS80A10 composition (see also Manning et al., 1980):

$$3NaAlSi_4O_{10} + 3F_2O_{-1} \Leftrightarrow Na_3AlF_6 + 2Al^{3+} + 6Q^3 + 6Q^4. \quad (11)$$

Equivalent expressions could be written for mixed (O,F)-complexes such as $Na(Na_3AlF_5O)$, for example.

Although formation of cryolite-like complexes in melts near meta-aluminosilicate composition results in depolymerization of the aluminosilicate network, in peralkaline aluminosilicate melts with (Na-Al) > $2/3Na_3AlF_6$, formation of cryolite-like complexes could actually result in polymerization of the aluminosilicate. Consider, for example, a melt composition with 50 mol.% NS80A10 ($NaAlSi_4O_{10}$) and 50 mol.% NS80A0 ($Na_2Si_4O_9$). Such a composition is equivalent to NS80A5. Solution of F in such a melt to form a complex of Na_3AlF_6 stoichiometry can be expressed as:

$$NaAlSi_4O_{10} + Na_2Si_4O_9 + 3F_2O_{-1} \Leftrightarrow Na_3AlF_6 + 8Q^4. \quad (12)$$

Equation 12 illustrates that solution of F to form Al-F complexes in peralkaline aluminosilicate melts can, in fact, result in aluminosilicate melt polymerization. This is because some of the network-modifying Na^+ is scavenged from the aluminosilicate to form cryolite-like complexes in a manner conceptually similar to NaF complexing discussed above.

5. SUMMARY

In summary, solution mechanisms of F in aluminosilicate melts depend significantly on silicate melt composition. Multiple F-complexes can form. Their effect on the aluminosilicate melt structure depends primarily on the type of F-complex, the Al-content and Na/Al-ratio of the melt.

Transport properties of silicate melts are sensitive to melt structure (Bockris et al., 1956; Riebling, 1966; Luth, 1988a,b; Neuville and Richet, 1991; Toplis and Dingwell, 1996). Several wt.% F reduces the viscosity of felsic aluminosilicate melts such as, for example, $NaAlSi_3O_8$, by several orders of magnitude and in this regard resembles the effect of H_2O (Dingwell et al., 1985). In contrast, the viscosity of depolymerized melts such as $CaMgSi_2O_6$ is barely affected by dissolved fluorine (Dingwell, 1989). These observations are consistent with fluorine solution mechanisms in silicate melts being composition-dependent (Carroll and Webster, 1994). In highly polymerized aluminosilicate melts, dissolved fluorine breaks bridging oxygen bonds, thus causing depolymerization and decreased viscosity as well as probably an increase in values of other

transport properties such as diffusivity and conductivity. The magnitude of any of these effects of dissolved F is likely to decrease as a melt becomes increasingly depolymerized because increasing depolymerization results in decreasing effects on melt structure of dissolved fluorine.

Solution of fluorine in silicate melts results in liquidus temperature depression. However, the extent of this temperature depression depends on the composition of the silicate melts. For highly polymerized melts such as $NaAlSi_3O_8$ it can be as much as 200–300°C, whereas for depolymerized materials such as, for example, $CaMgSi_2O_6$, the liquidus temperature depression is on the order of 100°C for F-saturated melts (Wyllie and Tuttle, 1961; van Groos and Wyllie, 1967; Luth, 1988a). It is likely that these differences result from different solution behavior of F in the melt. For highly polymerized aluminosilicate melts, the dissolved F results in significant structural changes of the aluminosilicate network (i.e., Eqns. 11–12). In depolymerized melts such as $CaMgSi_2O_6$, for example, formation of simple, perhaps isolated fluorine-clusters has a lesser effect on the melt structure and, therefore, causes less of a liquidus temperature depression.

Fluorine in silicate melts also tends to cause changes in liquidus phase relations. For example, the liquidus volumes of depolymerized silicates tend to expand relative to more polymerized materials (e.g., olivine vs. pyroxene and pyroxene vs. silica phases or plagioclase) (Foley et al., 1986; Luth 1988a). Depolymerization of silicate melts is coupled with a decrease in silica activity. Thus for melt compositions where solution of fluorine causes melt depolymerization (i.e., highly polymerized aluminosilicate melts), these changes in liquidus phase relations would be expected. Furthermore, in haplogranitic melt systems (feldspar + quartz), the liquidus volumes of feldspar phases shrink relative to that of quartz as fluorine is added to the melt (Manning, 1981; Manning et al., 1980). This observation is consistent with the formation of alkali-Al-F-complexes (e.g., Eqns. 10–12) in such melts thus reducing the activity of alkali aluminosilicate minerals such as feldspar.

Acknowledgments—Detailed and constructive reviews by J. Webster, G. Morgan, and an anonymous reviewer are greatly appreciated. This research was conducted with partial support from NSF grants EAR-9901886 and an REU grant from NSF to the Carnegie Institution of Washington. The NMR laboratory is supported in part by the W. M. Keck Foundation.

Associate editor: F. J. Ryerson

REFERENCES

Abragam A. (1961) The Principles of Nuclear Magnetism. Oxford University Press.

Bell R. J. and Dean P. (1972) Localization of phonons in vitreous silica and related glasses. *InInt. Conf. on Phys. Non-Cryst. Solids, 3* (ed. D. a. B. Ellis), pp. 443–452. Wiley-Intersciences.

Bockris J. O. M., Tomlinson J. W., and White J. L. (1956) The structure of liquid silicates. *Trans. Faraday Soc.* **52,** 299–311.

Brawer S. A. and White W. B. (1975) Raman spectroscopic investigation of the structure of silicate glasses. I. The binary silicate glasses. *J. Chem. Phys.* **63,** 2421–2432.

Brawer S. A. and White W. B. (1977) Raman spectroscopic investigation of the structure of silicate glasses. II. The soda-alkaline earth-alumina ternary and quaternary glasses. *J. Non-Cryst. Solids* **23,** 261–278.

Brown G. E., Gibbs G. V., and Ribbe P. H. (1969) The nature and variation in length of the Si-O and Al-O bonds in framework silicates. *Am. Mineral.* **54,** 1044–1061.

Buckermann W.-A., Muller-Warmuth W., and Frischat G. H. (1992) A further ^{29}Si MAS NMR study on binary alkali silicate glasses. *Glasstechn. Ber.* **65,** 18–21.

Carroll M. R. and Webster J. D. (1994) Solubilities of sulfur, noble gases, nitrogen, chlorine, and fluorine in magmas. *InVolatiles in Magmas, Vol. 30* (eds. M. R. Carroll and J. L. Holloway), pp. 231–280. Mineralogical Society of America.

Daniel I., Gillet P., Poe B. T., and McMillan P. F. (1995) In-situ high-temperature Raman spectroscopic studies of aluminosilicate liquids. *Phys. Chem. Mineral.* **22,** 74–86.

Dingwell D. B. (1987) Melt viscosities in the system $NaAlSi_3O_8$-H_2O-F_2O_{-1}. In *Magmatic Processes: Physicochemical Principles* (ed. B. O. Mysen), pp. 423–432.

Dingwell D. B. (1989) Effect of fluorine on the viscosity of diopside liquid. *Am. Mineral.* **74,** 333–338.

Dingwell D. B., Scarfe C. M., and Cronin D. J. (1985) The effect of flourine on viscosities in the system Na_2O-Al_2O_3-SiO_2: Implications for phonolites, trachytes and rhyolites. *Am. Mineral.* **70,** 80–87.

Dingwell D. B. and Webb S. L. (1990) Relaxation in silicate melts. *Eur. J. Mineral.* **2,** 427–449.

Duncan T. M., Douglass D. C., Csenscits R., and Walker K. L. (1986) Study of fluorine in silicate glasses with ^{19}F nuclear magnetic resonance spectroscopy. *J. Appl. Phys.* **60,** 130–136.

Engelhardt G. and Michel D. (1987) High-resolution Solid-state NMR of Silicates and Zeolites485 pp. Wiley.

Farnan I. and Stebbins J. F. (1990) A high temperature ^{29}Si investigation of solid and molten silicates. *J. Am. Ceram. Soc.* **112,** 32–39.

Foley S. F., Taylor W. R., and Green D. H. (1986) The effect of fluorine on phase relationships in the system $KAlSiO_4$-Mg_2SiO_4-SiO_2 at 28 kbar and the solution mechanism of fluorine in silicate melts. *Contrib. Mineral. Petrol.* **93,** 46–55.

Fukumi K., Hayakawa J., and Komiyama T. (1990) Intensity of Raman band in silicate glasses. *J. Non-Cryst. Solids* **119 (***3***),** 297–302.

Furukawa T., Fox K. E., and White W. B. (1981) Raman spectroscopic investigation of the structure of silicate glasses. III. Raman intensities and structural units in sodium silicate glasses. *J. Chem. Phys.* **153,** 3226–3237.

Geisinger K. L., Gibbs G. V., and Navrotsky A. (1985) A molecular orbital study of bond length and bond angle variations in framework structures. *Phys. Chem. Minerals* **11,** 266–283.

Gilbert B., Mamantov G., and Begun G. M. (1975) Raman spectra of aluminum fluoride containing melts and the ionic equilibrium in molten cryolite type mixtures. *J. Chem. Phys.* **62,** 950–955.

Hamilton W. C. (1965) Significance of the crystallographic R-factor. *Acta Cryst.* **18,** 502–510.

Kiczenski T. J. and Stebbins J. F. (2002) Fluorine sites in calcium and barium oxyfluorides: F-19 NMR of crystalline model compounds and glasses. *J. Non-Cryst. Solids* **306,** 160–168.

Knoche R., Dingwell D. B., Seifert F. A., and Webb S. L. (1994) Non-linear properties of supercooled liquids in the system Na_2O-SiO_2. *Chem. Geol.* **116,** 1–16.

Kohn S. C., Dupree R., Mortuza M. G., and Henderson C. M. B. (1991) NMR evidence for five- and six-coordinated aluminum fluoride complexes in F-bearing aluminosilicate glasses. *Am. Mineral.* **76,** 309–312.

Kreinbrink A. T., Sazavsky C. D., Pyrz J. D., Nelson D. G. A., and Honkonen R. S. (1990) Fast-magic-angle-spinning ^{19}F NMR in inorganic fluorides and fluoridated apatitic surfaces. *J. Magn. Reson.* **88,** 267–276.

Kushiro I. (1969) The system forsterite-diopside-silica with and without water at high pressures. *Am. J. Sci.* **267-A,** 269–294.

Lasaga A. C. (1982) Optimization of CNDO for molecular orbital calculation on silicates. *Phys. Chem. Minerals* **8,** 36–46.

Lee S. K. and Stebbins J. F. (1999) The degree of aluminum avoidance in aluminum silicate glasses. *Am. Mineral.* **84,** 937–945.

Liu Y. and Nekvasil H. (2001) Ab initio study of possible fluorine-bearing four- and five-fold coordinated Al species in aluminosilicate glasses. *Am. Mineral.* **86,** 491–497.

Liu Y, Tossell J. A (2003) Possible Al-F bonding environment in F-bearing. Na-aluminosilicate glasses: From calculation of ^{19}F NMR shifts. *J. Phys. Chem. B* **107,** 11286–11289.

Long D. A. (1977) Raman Spectroscopy. McGraw-Hill.

Luth R. W. (1988a) Effects of F on phase equilibria and liquid structure in the system $NaAlSiO_4$-$CaMgSi_2O_6$-SiO_2. *Am. Mineral.* **73,** 306–312.

Luth R. W. (1988b) Raman spectroscopic study of the solubility mechanisms of F in glasses in the system CaO-CaF_2-SiO_2. *Am. Mineral.* **73,** 297–305.

Maekawa H., Maekawa T., Kawamura K., and Yokokawa T. (1991a) The structural groups of alkali silicate glasses determined from ^{29}Si MAS-NMR. *J. Non-Cryst. Solids* **127 (***1***),** 53–64.

Maekawa H., Maekawa T., Kawamura K., and Yokokawa T. (1991b) ^{29}Si MAS NMR investigation of the Na_2O-Al_2O_3-SiO_2 glasses. *J. Phys. Chem.* **95,** 6822–6827.

Manning D. A. C. (1981) The effect of fluorine on liquidus phase relationships in the system Qz-Ab-Or with excess water at 1 kb. *Contrib. Mineral. Petrol.* **76,** 206–215.

Manning D. A. C., Hamilton C. M. B., Henderson C. M. B., and Dempsey M. J. (1980) The probable occurrence of interstitial Al in hydrous F-bearing and F-free aluminosilicate melts. *Contrib. Mineral. Petrol.* **75,** 257–262.

Matson D. W., Sharma S., and Philpotts J. A. (1986) Raman spectra of some tectosilicates and glasses along the orthoclase-anorthite and nepheline-anorthite joins. *Am. Mineral.* **71,** 694–704.

McMillan P. (1984) Structural studies of silicate glasses and melts—applications and limitations of Raman spectroscopy. *Am. Mineral.* **69,** 622–644.

McMillan P. F. and Wolf G. H. (1995) Vibrational spectroscopy of silicate liquids. *InStructure, Dynamics and Properties of Silicate Melts, Vol. 35* (eds. J. F. Stebbins, P. F. McMillan, and D. B. Dingwell), pp. 247–315. Mineralogical Society of Washington.

McMillan P. F., Wolf G. H., and Poe B. T. (1992) Vibrational spectroscopy of silicate liquids and glasses. *Chem. Geol.* **96,** 351–366.

McMillan P. F., Poe B. T., Gillet P., and Reynard B. (1994) A study of SiO_2 glass and supercooled liquid to 1950 K via high-temperature Raman spectroscopy. *Geochim. Cosmochim. Acta* **58,** 3653–3664.

Merzbacher C., Sherriff B. L., Hartman S. J., and White W. B. (1990) A high-resolution ^{29}Si and ^{27}Al NMR study of alkaline earth aluminosilicate glasses. *J. Non-Cryst. Solids* **124,** 194–206.

Miller J. M. (1996) Fluorine-19 magic angle spinning NMR. *Progr. Nucl. Magn. Resonance* **28,** 255–281.

Murdoch J. B., Stebbins J. F., and Carmichael I. S. E. (1985) High-resolution ^{29}Si NMR study of silicate and aluminosilicate glasses: The effect of network-modifying cations. *Am. Mineral.* **70,** 332–343.

Mysen B. O. (1995) Experimental, in-situ, high-temperature studies of properties and structure of silicate melts relevant to magmatic temperatures. *Eur. J. Mineral.* **7,** 745–766.

Mysen B. O. (1997) Aluminosilicate melts: Structure, composition and temperature. *Contrib. Mineral. Petrol.* **127,** 104–118.

Mysen B. O. (1999) Structure and properties of magmatic liquids: From haplobasalt to haploandesite. *Geochim. Cosmochim. Acta* **63,** 95–112.

Mysen B. O. (2003) Physics and chemistry of silicate glasses and melts. *Eur. J. Mineral.* **15,** 781–802.

Mysen B. O, Virgo D (1985) Interactions between fluorine and silica in quenched melts on the joins SiO_2-AlF_3 and SiO_2-NaF determined by Raman spectroscopy. *Phys. Chem. Minerals* **12,** 77–85.

Mysen B. O. and Frantz J. D. (1992) Raman spectroscopy of silicate melts at magmatic temperatures: Na_2O-SiO_2, K_2O-SiO_2, and Li_2O-SiO_2 binary compositions in the temperature range 25°–1475°C. *Chem. Geol.* **96,** 321–332.

Mysen B. O. and Frantz J. D. (1993) Structure of silicate melts at high temperature: In-situ measurements in the system BaO-SiO_2 to 1669°C. *Am. Mineral.* **78,** 699–1669.

Mysen B. O. and Frantz J. D. (1994a) Structure of haplobasaltic liquids at magmatic temperatures: In-situ, high-temperature study of melts on the join $Na_2Si_2O_5$-$Na_2(NaAl)_2O_5$. *Geochim. Cosmochim. Acta* **58,** 1711–1733.

Mysen B. O. and Frantz J. D. (1994b) Alkali silicate glass and melt structure in the temperature range 25–1651°C at atmospheric pressure and implications for mixing behavior of structural units. *Contrib. Mineral. Petrol.* **117,** 1–14.

Mysen B. O. and Cody G. D. (2001) Silicate–phosphate interaction in silicate glasses and melts. II. Quantitative, high-temperature structure of P-bearing alkali aluminosilicate melts. *Geochim. Cosmochim. Acta* **65,** 2413–2431.

Mysen B. O., Virgo D., and Kushiro I. (1981) The structural role of aluminum in silicate melts—A Raman spectroscopic study at 1 atmosphere. *Am. Mineral.* **66,** 678–701.

Mysen B. O., Finger L. W., Seifert F. A., and Virgo D. (1982) Curve-fitting of Raman spectra of amorphous materials. *Am. Mineral.* **67,** 686–696.

Mysen B. O., Lucier A., and Cody G. D. (2003) The structural behavior of Al^{3+} in peralkaline melts and glasses in the system Na_2O-Al_2O_3-SiO_2. *Am. Mineral.* **88,** 1668–1678.

Neuville D. R. and Mysen B. O. (1996) Role of aluminum in the silicate network: In-situ, high-temperature study of glasses and melts on the join SiO_2-$NaAlO_2$. *Geochim. Cosmochim. Acta* **60,** 1727–1738.

Neuville D. R. and Richet P. (1991) Viscosity and mixing in molten (Ca,Mg) pyroxenes and garnets. *Geochim. Cosmochim. Acta* **55,** 1011–1020.

Osborn E. F, Muan A (1960) Phase equilibrium diagrams for ceramists. Plate 4. The system Na_2O-Al_2O_3-SiO_2. American Ceramic Society, Columbus, OH.

Pearce M. L. (1964) Solubility of carbon dioxide and variation of oxygen ion activity in soda-silicate melts. *J. Am. Ceram. Soc.* **47,** 342–347.

Richet P. and Bottinga Y. (1986) Thermochemical properties of silicate glasses and liquids: A review. *Rev. Geophys.* **24,** 1–26.

Richet P., Ingrin J., Mysen B. O., Courtial P., and Gillet P. (1994) Premelting effects in minerals; an experimental study. *Earth Planet. Sci. Lett.* **121 (***3–4***),** 589–600.

Riebling E. F. (1966) Structure of molten sodium aluminosilicate liquids containing at least 50 mol. % SiO_2 at 1500°C. *J. Chem. Phys.* **44,** 2857–2865.

Sato R. K., McMillan P. F., Dennison P., and Dupree R. (1991) A structural investigation of high alumina glasses in the CaO-Al_2O_3-SiO_2 system via Raman and magic angle spinning nuclear magnetic resonance spectroscopy. *Phys. Chem. Glasses* **32 (***4***),** 149–160.

Schaller T., Dingwell D. B., Keppler H., Knoller W., Merwin L., and Sebald A. (1992) Fluorine in silicate glasses: A multinuclear magnetic resonance study. *Geochim. Cosmochim. Acta* **56,** 701–707.

Seifert F. A., Mysen B. O., and Virgo D. (1982) Three-dimensional network structure in the systems SiO_2-$NaAlO_2$, SiO_2-$CaAl_2O_4$ and SiO_2-$MgAl_2O_4$. *Am. Mineral.* **67,** 696–711.

Stebbins J. F. (1995) Dynamics and structure of silicate and oxide melts; nuclear magnetic resonance studies. *InStructure, Dynamics and Properties of Silicate Melts, Vol. 32* (eds. J. F. Stebbins, P. F. McMillan, and D. B. Dingwell), pp. 191–246. Mineralogical Society of America.

Stebbins J. F. and Zeng Q. (2000) Cation ordering at fluoride sites in silicate glasses: A high-resolution ^{19}F NMR study. *J. Non-Cryst. Solids* **262,** 1–5.

Stebbins J. F., Kroeker S., Lee S. K., and Kiczenski T. J. (2000) Quantification of five- and six-coordinated aluminum ions in aluminosilicate and fluoride-containing glasses by high-field, high-resolution ^{27}Al NMR. *J. Non-Cryst. Solids* **275,** 1–6.

Taylor M. and Brown G. E. (1979) Structure of mineral glasses. II. The SiO_2-$NaAlSiO_4$ join. *Geochim. Cosmochim. Acta* **43,** 1467–1475.

Toplis M. J. and Dingwell D. W. (1996) The variable influence of P_2O_5 on the viscosity of melts of differing alkali/aluminum ratio: Implications for the structural role of phosphorus in silicate melts. *Geochim. Cosmochim. Acta* **60,** 4107–4121.

Tossell J. A. (1993a) Theoretical studies of the speciation of Al in F-bearing aluminosilicate glasses. *Am. Mineral.* **78,** 16–22.

Tossell J. A. (1993b) A theoretical study of the molecular basis of the Al avoidance rule and of the spectra; characteristics of Al-O-Al linkages. *Am. Mineral.* **78,** 911–920.

Urbain G., Bottinga Y., and Richet P. (1982) Viscosity of liquid silica, silicates and aluminosilicates. *Geochim. Cosmochim. Acta* **46,** 1061–1072.

Van Groos K. and Wyllie P. J. (1967) Melting relationships in the system $NaAlSi_3O_8$-NaF-H_2O to 4 kb pressure. *J. Geol.* **76,** 50–70.

Virgo D., Mysen B. O., and Kushiro I. (1980) Anionic constitution of 1-atmosphere silicate melts: Implications of the structure of igneous melts. *Science* **208,** 1371–1373.

Wyllie P. J. and Tuttle O. F. (1961) Experimental investigation of silicates containing two volatile components. II. The effects of NH_3 and HF in addition to water on the melting temperatures of granite and albite. *Am. J. Sci.* **259,** 128–143.

Yamamoto K., Nakanishi T., Kasahara H., and Abe K. (1983) Raman scattering of SiF_4 molecules in amorphous fluorinated silicon. *J. Non-Cryst. Solids* **59-60,** 213–216.

Zeng Q. and Stebbins J. F. (2000) Fluoride sites in aluminosilicate glasses: High-resolution ^{19}F NMR results. *Am. Mineral.* **85,** 863–867.